AD A113354

READ INSTRUCTIONS
BEFORE COMPLETING FORM

1. Report Number	2. Govt Accession No.	3. Recipient's Catalog Number
EOARD-TR-82-9	AD-A113354	

4. Title (and Subtitle)	5. Type of Report & Period Covered
An experimental and numerical study of an air-to-air heat exchanger using liquid reservoir variable conductance heat pipes	Final Scientific Report 1 Feb 81 - 31 Jan 82
	6. Performing Org. Report Number

7. Author(s)	8. Contract or Grant Number
S. DROUILHET & J-M. BUCHLIN	Grant AFOSR 81-120

9. Performing Organization Name and Address	10. Program Element, Project, Task Area & Work Unit Numbers
von Karman Institute for FluidDynamics Chaussée de Waterloo, 72 B-1640 Rhode Saint Genèse, Belgium	P.E. 61102F Proj/Task 2301/D1 W.U. 123

11. Controlling Office Name and Address	12. Report Date
European Office of Aerospace Research and Development/LNT Box 14 FPO New York 09510	
	13. Number of Pages 94

14. Monitoring Agency Name and Address	15.
European Office of Aerospace Research and Development/LNT Box 14 FPO New York 09510	

16. & 17. Distribution Statement

Approved for public release; distribution unlimited.

18. Supplementary Notes

19. Key Words

Heat exchanger;Heat pipes;Thermal behaviour modelling; Air conditioning-application

20. Abstract
This report documents a study of a prototype air-to-air heat exchanger of which the thermal conductivity is governed by the reservoir temperature of the heat pipes. The work is introduced with a brief review of the basic operating principles of heat pipes and of the various existing schemes for variable conductance.
An experimental facility, incorporating a computerized data acquisition system, was developed to investigate the steady state performance characteristics of the heat exchanger over a wide range of air inlet temperatures, mass flow rates, and reservoir temperatures. Some tests were conducted imposing a single operating temperature on all of the heat pipes, while in others the heat pipe rows were allowed to operate independently. The results are expressed in terms of heat exchanger effectiveness versus normalized reservoir temperature for various values of the ratio of the mass flow rates of the air streams. Conclusions are drawn as to the internal behaviour of this type of heat pipes under various operating regimes.
An original computer model is presented which combines a quasi analytical solution for the air and fin temperature profiles in the heat exchanger with a heat pipe simulation routine based on the hydrodynamic equations involved in the working fluid cycle. Computational results are shown, and a brief comparison with the experiments is made. Possible modifications that would improve the accuracy and the versatility of the program are discussed.

EOARD-TR-82-9

This report has been reviewed by the EOARD Information Office and is releasable to the National Technical Information Service (NTIS). At NTIS it will be releasable to the general public, including foreign nations.

This technical report has been reviewed and is approved for publication.

WINSTON K. PENDLETON
Lt Colonel, USAF
Chief Scientist

GORDON L. HERMANN
Lt Colonel, USAF
Deputy Commander

Accession For		
NTIS GRA&I		☒
DTIC TAB		☐
Unannounced		☐
Justification		
By		
Distribution/		
Availability Codes		
Dist	Avail and/or Special	
A		

DTIC COPY INSPECTED 2

EOARD-TR-82-9

TABLE OF CONTENTS

ACKNOWLEGEMENTS

ABSTRACT

This report documents a study of a prototype air-to-air heat exchanger of which the thermal conductivity is governed by the reservoir temperature of the heat pipes. The work is introduced with a brief review of the basic operating principles of heat pipes and of the various existing schemes for variable conductance.

An experimental facility, incorporating a computerized data acquisition system, was developed to investigate the steady state performance characteristics of the heat exchanger over a wide range of air inlet temperatures, mass flow rates, and reservoir temperatures. Some tests were conducted imposing a single operating temperature on all of the heat pipes, while in others the heat pipe rows were allowed to operate independently. The results are expressed in terms of heat exchanger effectiveness versus normalized reservoir temperature for various values of the ratio of the mass flow rates of the air streams. Conclusions are drawn as to the internal behaviour of this type of heat pipes under various operating regimes.

An original computer model is presented which combines a quasi-analytical solution for the air and fin temperature profiles in the heat exchanger with a heat pipe simulation routine based on the hydrodynamic equations involved in the working fluid cycle. Computational results are shown, and a brief comparison with the experiments is made. Possible modifications that would imporve the accuracy and the versitility of the program are discussed.

LIST OF SYMBOLS

c_p	specific heat of air at constant pressure	J/kg°C
d_p	external diameter of heat pipe	m
e	plate thickness	m
f	friction coefficient	
g	gravitational constant	m/s^2
h	total convective heat transfer coefficient	W/m^2°C
k	thermal conductivity	W/m°C
ℓ	length of heat pipe section	m
$\dot{m}$	mass flow rate	kg/s
p	static pressure	N/m^2
s	fin spacing	m
t	fin thickness	m
u	bulk velocity	m/s
w	width of heat exchanger	m
x	flow direction	m
y	lateral direction	m
z	heat pipe axis	m
$\underline{A}$	coefficient matrix in the numerical solution of the heat exchanger node temperatures	
$\underline{B},\underline{C}$	coefficient vectors in the numerical solution	
A_{HX}	wetted area in one side of heat exchanger	m^2
A_n	normal flow area	m^2
A_f	projected fin area	m^2
MR	mass flow ratio	

N_p	number of heat pipes	
Q	heat transfer rate	W
T	temperature	°C, °K

ϵ	effectiveness	
ϕ	heat flux in a row of heat pipes	W
Φ	normalized heat flux in a row of heat pipes	°C/m
τ	wall shear stress	N/m
ρ	density	kg/m
X	non dimensionalized x coordinate	
χ	normalized platelet length	

Subscripts

a	"adiabatic" or "air"
c	"condenser"
e	"evaporator"
i	platelet number, node number
ℓ	"liquid"
n	"normalized"
R	"reservoir"
v	"vapour"
0	"leading edge of a platelet"
1	"trailing edge of a platelet"
∞	"upstream of the heat exchanger"

Superscript

| i | platelet number |

LIST OF FIGURES

1. INTRODUCTION

A problem that has always been associated with the design of effective air-to-air heat exchangers is their high bulk and weight, due to the very large surfaces required to transfer significant amounts of heat from one airstream to another. The birth and rapid growth of heat pipe technology in the 1960s led to the eventual development of more compact heat exchangers taking advantage of the very high thermal conductivity of these devices. The continued development of such heat exchangers brought the promise of many new applications in the fields of energy conservation and air-conditioning. At the same time, however, a significant limitation of existing heat pipe heat exchangers became apparent, namely, a lack of controllability. While it is undisputably a high performance heat transfer device, the standard heat pipe's thermal conductivity is highly dependent on its operating temperature and on the thermal load placed across it; in other words, the overall heat transfer coefficient is a function of the heat sink and source conditions. With the standard heat pipe, it is impossible to adjust this heat transfer coefficient, and therefore impossible to regulate the heat flux in a heat exchanger using them.

This limitation poses problems for heat recovery and temperature control applications. In heat recovery systems, in which waste heat is recovered from exhausted air (or process gases) and used to heat cold incoming air, it is desirable to maximize the heat transfer rate, i.e., the heat exchanger's effectiveress. Uncontrollable heat pipe heat exchangers work, however, at an effectiveness which is not necessarily their optimum. The working point is passively determined by the temperature and mass flow rate of the two airstreams. Such heat exchangers are also inadequate to meet the requirements of air-conditioning systems, where one must control the exit temperature of one of the airstreams, since the air exit conditions are uniquely determined by the inlet conditions. This lack of

controllability is the motive behind the research on variable
conductance heat pipe heat exchangers. Much work has been
done to develop both passively and actively controlled heat
pipes. Some of the resulting systems will be mentioned in
the following sections.

This report documents both an experimental and numeri-
cal study of a prototype variable conductance heat pipe (VCHP)
heat exchanger based on the principle of operating temperature
modulation. This particular design, which makes use of liquid
reservoirs of excess working fluid, offers the possibility of
heat flux maximization and temperature control without moving
parts. The objectives of this study are to determine the steady
state performance characteristics of this heat exchanger over
a wide range of operating conditions and to apply heat pipe
theory to develop a numerical model of the heat exchanger
capable of predicting temperature profiles and heat flux for
specified air inlet conditions. Such a model would be useful
as a tool for both the design and control of this type of heat
exchanger.

2. HEAT PIPE PRINCIPLES

2.1 The standard heat pipe

Before discussing the details of the liquid reservoir VCHP, it is useful to review the fundamental principles of heat pipes. The heat pipe is a high performance heat transfer device, able to transfer heat at high rates over considerable distances with almost no temperature drop. In its basic form the heat pipe consists of a sealed tube lined with a porous capillary wick that is saturated with a volatile fluid as shown in figure 1. Heat absorbed by the evaporator zone vaporizes the fluid; vapour flows to the other end where it condenses, giving up the heat. The fluid cycle is then completed as the condensed fluid flows in the wick back to the evaporator. The axial heat transfer is thus equal to the mass circulation rate times the latent heat of vaporization of the working fluid.

Frequently the evaporator and condenser sections are separated by an adiabatic zone, where there is no heat flux into or out of the pipe. A heat pipe can, in principle, operate with the evaporator above the condenser as shown in figure 1, in which case the capillary head generated in the wick must overcome the gravitational head, but in many cases the evaporator is intentionally placed below the condenser so that these two forces work together, which facilitates the return of the condensate to the evaporator.

What appears to be a simple device actually involves a complex set of thermal and hydrodynamic processes, which have made it difficult for researchers to draw firm conclusions about the exact nature of the heat transfer processes in a particular heat pipe for a given set of heat source and sink conditions. What has been determined is that the heat pipe's performance is bounded by an envelope of limiting conditions as shown in figure 2.

2.2 Limits to heat transfer

The range of vapour temperature (also called opera-
ting temperature) over which a particular heat pipe functions
is determined principally by the working fluid used. At the
low end of this range, fluid viscosity imposes a limit on the
heat transfer capacity of the heat pipes, as shown in figure 2.

For slightly higher operating temperatures, what is
called the sonic limit is the dominant limiting factor. It
can be shown analytically that there is a correspondence be-
tween constant area flow in a heat pipe with mass addition
(evaporator) and removal (condenser) and constant mass flow
in a converging-diverging nozzle. Consequently, just as there
is a sonic (Mach = 1) limitation on the flow velocity through
a nozzle, there is a similar limit on the flow velocity through
the adiabatic section of the heat pipe.

Another phenomenon which may limit heat flux over a
certain range of operating temperature is liquid entrainment
in the vapour. In a heat pipe, the vapour and the liquid
generally flow in opposite directions. Since they are in
contact at the wick surface (if the wick is saturated), this
sets up a mutual drag at the vapour-liquid interface. If the
relative velocity between the liquid and vapour becomes too
great, the interface becomes unstable and droplets of liquid
will be torn from the wick and entrained in the vapour. Since
this liquid never reaches the evaporator, it cannot contribute
to the heat transferred by the heat pipe. Thus, the maximum
axial heat transfer is no longer equal to the maximum fluid
circulation rate times the latent heat of vaporization, but
is some lower value.

The fact that there exists a maximum capillary head
for any wick-fluid combination results in a hydrodynamic limit
on heat pipe capacity. In order for the heat pipe to operate,
the following pressure balance equation must be satisfied

between any two points along the heat pipe :

$$\Delta p_{c,max} + \Delta p_g \geqslant \Delta p_\ell + \Delta p_v \qquad (2.1)$$

where $\Delta p_{c,max} \equiv$ maximum capillary head

Δp_g gravitational head acting on liquid (evaporator assumed to be positioned below the condenser)

Δp_ℓ pressure drop in liquid due to viscous drag

Δp_v pressure drop in vapour due to viscous drag and mass transfer.

This equation states that for any fluid path defined by two points along the heat pipe, the sum of the driving forces (capillary head and gravitational head) must be equal to the sum of the pressure losses undergone by the liquid and vapour. These pressure losses are dependent on the fluid circulation rate (and hence the thermal load), whereas the maximum capillary head and the gravitational head are essentially independent of load. When the load increases so that the two sides of the equation are equal anywhere along the heat pipe, the capillary pumping limited has been reached.

Finally, there exists a boiling (burnout) limit which corresponds to the formation of a stable vapour film within the wick due to the excessively rapid production of bubbles, whose escape is inhibited by the wick structure. This condition tends to arise for high operating temperatures where there is a large temperature differential across the evaporator wick.

In all cases, the heat pipe operates within the area bounded by the curves shown in figure 2. For the standard heat pipe, the actual operating point is determined solely by the heat source and sink temperatures. The goal of variable conductance designs is to be able to displace this point at will, and in some cases even to change the shape of the operating envelope defined by these limiting conditions.

2.3 Variable conductance heat pipes

For reasons already stated, the concept of variable conductance heat pipes was extensively developed beginning in the late 1960s. Most variable conductance designs employ a second fluid, an inert non-condensable gas, to act as a buffer to the heat transfer process. The inert gas, which in principle remains unmixed with the working fluid, is compressed into a reservoir at the condenser end of the heat pipe by the total pressure of the working vapour (Fig. 3). The non-condensable gas blocks a portion of the condenser whose length depends on the thermal load on the heat pipe. As the thermal load increases, the inert gas is further compressed, exposing more of the condenser to the working vapour, thus increasing the heat transfer rate and limiting variations in heat source and/or sink temperature.

The heat transfer rate may either be controlled passively, as just described, or actively, in which case the inert gas reservoir is heated or cooled in order to regulate more precisely the position of the vapour/gas interface and hence the effective length of the condenser section.

There exist other schemes for variable conductance heat pipes; these are mostly the so called vapour flow modulation or liquid flow modulation types, where a throttling mechanism is placed either in the vapour or liquid phase of the flow circuit. This may consist of a variable orifice through which the vapour passes on its way from the evaporator to the condenser, or it may be some sort of controllable interruption or impediment to condensate flow in the wick. Unlike the non-condensable gas reservoir type of VCHP, both of these latter concepts require the use of moving parts.

All of the above mentioned methods of heat pipe control have several properties in common. First, the quantity of working fluid present in the heat pipe remains

constant regardless of the control setting. Secondly, these
control systems can only _attenuate_ the heat flux from some
maximum value attainable were the control system not present.
These systems, then, meet the needs of only one class of
applications discussed in the introduction, namely temperature
control, and this only when the thermal potential placed
across the heat pipes is always greater than or equal to the
required heat transfer.

2.4 Liquid reservoir variable
conductance heat pipes

The liquid reservoir VCHP is based on a different
principle than the proceeding types. It uses no direct inter-
vention in the fluid circulation process to control heat flux;
instead, the thermal conductance is varied by modulating the
heat pipe's vapour temperature. Refering to the cutaway view
in figure 4, one sees that the evaporator end of each heat
pipe is connected to an unwicked reservoir capable of holding
condensed working fluid. Vapour can flow freely from the
reservoir to the heat pipe, or vice versa, whereas liquid
condensate can only run down from the heat pipe into the
reservoir, since the heat pipe is operated in the vertical
position. The heat pipe/reservoir combination contains slightly
more working fluid than is required to completely saturate the
wick; thus, a liquid/vapour interface always exists within the
reservoir. A possible exception is when the heat pipe is
functioning at a high heat transfer rate with a high reservoir
temperature, a situation in which reservoir dryout could occur.
Since heat pipe operation depends on the existence of pressure
differentials between the liquid and vapour phases in the eva-
porator and condensor, as well as pressure gradients within
each phase (as expressed by equation 2.1), it cannot truly be
said that the liquid and vapour phases are in equilibrium.
The variations in vapour pressure and temperature are so small,
however, that the vapour can be considered saturated everywhere

in the heat pipe and in the reservoir. Consequently, the operating temperature (and hence the operating pressure) is determined by the temperature of the liquid in the reservoir. For the experimental work described in this report, the assumption was made that due to the high conductivity of the copper reservoir walls, the externally measured reservoir temperature is approximately equal to the vapour temperature in the heat pipe.

Variable conductance is achieved in this context by variation of the reservoir temperature, which, by imposing an operating temperature and pressure on the heat pipe, causes a particular operating regime to be established by the interplay of thermal and hydrodynamic processes in the heat pipe. This operating regime, with its corresponding thermal conductivity, is characterized by the amount of fluid present in the heat pipe and by its circulation rate.

2.5 The prototype

The heat exchanger being investigated is shown schematically in figure 3 and its photograph appears in figure 4. It consists of an inline array of sixteen finned heat pipes, where each row of four heat pipes, transverse to the flow direction, has a single reservoir serving all of the heat pipes in that row. There is a divider plate located midway along the heat pipe which divides the heat exchanger into evaporator and condenser sections. As seen in the photograph, a short length of the divider plate is bent over at the ends, forming tabs which effectively block part of the heat exchanger face, thereby creating a short adiabatic zone between the evaporator (bottom) and condenser (top). A summary of the key heat exchanger dimensions, as well as the known and estimated heat pipe parameters is given in Appendices A and C.

3. THE EXPERIMENTAL INVESTIGATION

3.1 The test facility

To make optimum use of the VKI laboratory facilities, the heat pipe heat exchanger was adapted to the Institute's already existing solar energy test set-up (Ref. 1). The modified system, with the heat exchanger in place, is sketched in figure 6. The system consists simply of two open circuits, the hot air path passing through the evaporator side of the heat exchanger, the cold air path through the condenser side. Each circuit is equipped with a fixed speed blower, an orifice plate flow meter, and a valve to regulate the mass flow rate. The hot air circuit is equipped with an electrical resistance heater that has power settings of 2, 4 and 6 Kw. The cold air circuit is equipped with a water-to-air heat exchanger capable of cooling the air to approximately 15°C (depending on the water flow rate) before it passes through the condenser. All of the tests referred to in this report were conducted in the counterflow configuration.

As indicated in figure 6, the test facility is outfitted with a microprocessor-controlled data acquisition system linked to a mini-computer capable of doing real time data reduction. Both the microprocessor and the mini-computer control programs (Ref. 2) are adaptations of the programs used to perform data acquisition in the SUN experiments. The versions used for this study permit the scanning of up to 48 thermocouples as well as two pressure transducers, with a total acquisition time of about 30 seconds and a variable interval between acquisitions.

Temperature control of the liquid reservoirs was achieved in one of three different ways, depending on the type of test :

1.   All four reservoirs were placed in a large oil bath
(Fig. 7), whose temperature was maintained nearly uniform by
means of a rheostatically controlled electrical resistance
heater and a rotating agitator.

2.   All four reservoirs were placed in insulating sleeves to
effectively eliminate heat transfer between the reservoirs
and the surroundings.

3.   The reservoirs were placed in individual baths, one of
which contained heated oil as in case 1, while the other
three contained ice water. This permitting the testing of
the heat exchanger with only one row of heat pipes active
at a time.

3.2   Instrumentation of the heat exchanger

The heat exchanger was sandwiched between two coup-
ling sections, which were designed to provide a smooth transi-
tion of the flow in the 160 mm diameter circular ducting to
the rectangular flow section of the heat exchanger. Near the
inlet and outlet of each side of the heat exchanger there were
apertures in the coupling sections which gave access to the
test sections. The whole assembly consisting of heat exchanger
and coupling sections was mounted on a support designed for
testing the heat exchanger at 0°, 30°,45°, 60° and 90° from
the vertical. All measurements discussed in this report were
performed with the heat exchanger in the vertical position.

Static pressure taps were drilled in the walls of
the coupling sections opposite the test section apertures
(Fig. 7). A pressure transducer was connected to each pair
of taps to measure the pressure differential across the eva-
porator and condenser sections of the heat exchanger. Although
several types (Setra, Validyne) of transducers were used during
the course of experiments, they all had a high sensitivity
(range $\sim$ 70 mm H_2O) and they all gave an output on the order
of one volt, so as to be compatible with the data acquisition
system without the use of intermediate amplifiers.

Two types of probes were placed in the test sections, a vane anemometer to measure the velocity of the air stream and thermocouples to measure its temperature. A plexiglas sliding mechanism (Fig. B) was designed to hold the anemometer and seal the test section apertures, while allowing manual displacement of the probe in the y and z directions (x being the flow direction). All velocity measurements were made without heating or cooling or the airstream and the data acquisition system was not used. For the thermal measurements, thermocouples were placed at the inlet and outlet of both sides of the heat exchanger. A plate, through which were passed two thermocouple wires, was placed over the aperture at each inlet section. These thermocouple wires were drawn taut by fine copper wires which passed through the static pressure taps and were clamped there by the plastic pressure tubing. The wires were positioned such that the temperature sensitive thermocouple junctions were situated midway across the test section. This simple but effective system was adapted in order to minimize perturbation of the flow upstream of the heat exchanger.

In both the evaporator and condenser outlet test sections was placed a grid of fifteen thermocouples, arranged in five rows of three thermocouples (Fig. 9). The thermocouple heads protrude from hollow steel tubing, which can slide with respect to the mounting plate, thus permitting a degree of freedom in the lateral position of the thermocouple columns. For the tests described in this paper, the three columns (in each grid) of thermocouples were aligned with the spaces between the columns of heat pipes.

There were additional thermocouples connected to the data acquisition system. One of these was, of course, a reference, which was placed in an ice bath; the others measured the ambient air temperature and the external temperature of each reservoir.

3.3 Preliminary measurements :

flow characteristics

3.3.1 Velocity profiles

Velocity profile measurements were conducted for two reasons : first, to get an idea of the uniformity of the flow at the inlet and outlet of the heat exchangers, and second, to determine the optimal placement of the thermocouples at the outlet section.

It was found that when the probe was placed directly downstream of a column of heat pipes, the measured air velocity varied quite erratically as the probe was displaced in the z direction, indeed, falling to zero (or at least below the sensitivity threshold of the anemometer) at some points along the measurement line. We concluded from this that there remains a turbulent wake downstream of the heat exchanger behind each column of heat pipes in which the vane anemometer is unsuitable for velocity measurement. The non-uniformity of this wake (as indicated by the vane anemometer) may be due to a high degree of sensitivity, in the wake region, to small irregularities in fin geometry and spacing. This possibility is suggested by the fact that the lightweight fins had been deformed at various points on both faces of the heat exchanger due to previous mishandling. Due to the presence of these highly irregular wake regions, it was decided to represent the velocity profiles in the outlet section in terms of measurements made along lines in the streamplanes midway between the heat pipe columns. This was also the reason for positioning the thermocouple columns midway between the heat pipe wake regions.

The two dimensional inlet and outlet profiles were measured for the evaporator section with a mass flow rate of approximately .1 kg/s. At the inlet section there were

velocity gradients in both the vertical and lateral directions.
A careful examination of the heat exchanger assembly revealed
that the non-uniformity of the inlet velocity profile corres-
ponded to a misalignment of the air inlet pipe. The outlet
velocity profile, though based on a much sparser data field,
indicates that as the air passes through the heat exchanger,
a high degree of flow uniformization occurs in the lateral
direction, whereas the average vertical velocity gradients
tended to remain constant. This is intuitively comprehen-
sible; air that enters fins with velocity gradients in both
the y and z directions has a chance to redistribute itself
in a plane parallel to the fins, thereby reducing lateral
gradients, but not in a plane normal to the fins, once the
air is trapped between the fins. Hence, except for some
slight vertical flow redistribution that may take place im-
mediately upstream of the heat exchanger, the vertical velo-
city gradients are preserved. These findings lead one to
conclude that, although it may be difficult to achieve a
totally uniform flow field at the inlet, special attention
should be paid toward minimizing velocity gradients normal
to the fins.

The most important conclusion to be drawn from these
tests is that the outlet velocity profile was sufficiently
uniform (out of the wake zone) to justify a simple averaging
of all the temperatures given by the thermocouple grid to
determine the bulk temperature of the outlet air stream.

3.3.2 Pressure drop

As part of the preliminary testing program, a series
of measurements was conducted to determine the functional
relationship between the mass flow rate through the heat ex-
changer and the resulting pressure drop. This information is
used for two purposes :

1. During the thermal measurements, the mass flow rates are computed from the pressure drop across each side of the heat exchanger. This is a very direct method of flow metering, one which eliminates errors due to leaks at other points in the flow circuit, which in fact were found to be a problem in the SUN installation.

2. A derivation of the convective heat transfer coefficient in the heat exchanger, necessary for the computer model, is possible knowing the function relating mass flow rate to pressure drop.

We define the friction factor with the following equation, which relates the average component in the flow direction of the wall shear stress in the heat exchanger to the dynamic pressure of the air based on its bulk velocity in the inlet section

$$\tau = f \frac{\rho u^2}{2} \qquad (3.1)$$

where f = friction factor.

τ = average axial component of wall shear stress in the heat exchanger

ρ = air density

u = bulk velocity of air in inlet section

The mass flow rate through the heat exchanger is given by :

$$\dot{m} = \rho u A_n \qquad (3.2)$$

where A_n = cross sectional flow area (inlet section)

Taking the heat exchanger itself as a control volume, a force balance on the air gives

$$\Delta p A_n = \tau\, A_{HX} \tag{3.3}$$

where A_{HX} = heat exchange surface area.

Combining equations 3.1 and 3.3, one gets

$$u = \sqrt{\frac{2c}{\rho f}}\ \sqrt{\Delta p}$$

where $c = \dfrac{A_n}{A_{HX}}$. Substituting this into equation 3.2 gives

$$\dot{m} = A_n \sqrt{\frac{2\rho c}{f}}\ \sqrt{\Delta p} \tag{3.4}$$

The lengths of the evaporator and condenser sections are not exactly equal; there are different values for A_n and A_{HX}

$$A_n = \text{height} \times \text{width}$$
$$\left(A_n\right)_e = .24 \quad .13 = .0312\ m$$
$$\left(A_n\right)_e = .22 \quad .13 = .8286\ m$$

$$A_{HX} = 2\ (\text{number of fins})\ (\text{exposed fin area}) +$$
$$+ (\text{number of heat pipes})\ (\text{exposed pipe area})$$

$$A_{HX} = \frac{\ell}{s}\left[2\left(A_f - N_p\, \frac{\pi d_p^2}{4} \right) + N_p \pi d_p (s-t) \right]$$

ℓ = height of section

s = fin spacing

t = fin thickness

A_f = projected area of fin

N_p = number of heat pipes

d_p = diameter of heat pipes

$$\left(A_{HX}\right)_e = 4.23 \text{ m}^2$$

$$\left(A_{HX}\right)_c = 3.88 \text{ m}^2$$

Hence, $C = \dfrac{A_n}{A_{HX}} = .00738$ for both sides of the heat exchanger.

Figures 11 and 12 show the mass flow rate (as measured with a reference orifice plate flow meter, Ref. 3) plotted with respect to the square root of the pressure drop measured across the evaporator and condenser sections of the heat exchanger, respectively. These measurements showed very little random error and were highly repeatable. Clearly, the most striking feature of the data is its linearity above a certain threshold mass flow rate of about .04 kg/s. This means that in equation 3.4, the friction factor f can be considered constant in this range, provided a constant term is added to the right hand side of the equation to compensate for the fact that the extrapolation of the linear portion of the curve does not pass through the origin. There is no a priori reason that this must be so; indeed, the friction factor in any internal flow situation is a function of Reynolds number. It appears, however, that above a certain mass flow rate, the friction factor for this particular geometry achieves Reynolds number independence, as does the friction factor for turbulent flow in rough pipes.

A best fit to the points in the linear range gives the following expressions for mass flow rate.

Condenser

$$\dot{m} = .0142 \ \sqrt{\Delta p} - .0036 \quad [\Delta p] = Pa \tag{3.5a}$$

$$\dot{m} = .0444 \ \sqrt{\Delta p} - .0336 \quad [\Delta p] = mm \ H_2O \tag{3.5b}$$

$$\dot{m} = .202\ell_c \ \sqrt{\Delta p} - .0336 \quad [\Delta p] = mm \ H_2O \tag{3.5c}$$

$$[\ell_c] = meters$$

Evaporator

$$\dot{m} = .0150 \ \sqrt{\Delta p} - .0340 \quad [\Delta p] = Pa \tag{3.6a}$$

$$\dot{m} = .0471 \ \sqrt{\Delta p} - .0340 \quad [\Delta p] = mm \ H_2O \tag{3.6b}$$

$$\dot{m} = .0196\ell_c \ \sqrt{\Delta p} - .0340 \quad [\Delta p] = mm \ H_2O \tag{3.6c}$$

$$[\ell_e] = meters$$

The slope of these lines is equal to the grouping $A_n\sqrt{2_\rho c/f}$, from which f can be determined. The following values are found.

condenser : f = .078
evaporator : f = .074

Since the friction factor (assuming Reynolds independence) is only a function of flow geometry, it is reasonable to assume that the friction factor for both sides of the heat exchanger should be the same. For simplicity, then, we will use the average value f = .076.

3.4 Thermal measurements

3.4.1 Data acquisition and processing

Figure 12 is a close-up view of the data acquisition system (DAS), which rapidly gathers and processes all relevant pressure and temperature data. Figure 13 shows the heat exchanger mounted on its support, outfitted with thermocouples and pressure transducers, and connected to the DAS. During each acquisition cycle, the MEKII microprocessor feeds data to the PET minicomputer, where BASIC control program then performs calculations and prints out the results. What follows is a description of the calculations in the data reduction process.

Mass flow rate

The mass flow rates through the evaporator and condenser sections are computed on the basis of the pressure transducer output using equations 3.5c and 3.6c.

Heat transfer rate

The heat transfer rate between air streams is not measured directly. The measurements only allow the calculation of the heat given up by the hot air and the heat absorbed by the cold air. Since the heat pipes are connected to liquid reservoirs, which may act as either heat sources or sinks, these two heat transfer rates are not necessarily the same. They are given by the expressions

$$Q_e = \dot{m}_e c_p \left(T_{1,e} - T_{2,e} \right) \tag{3.7}$$

$$Q_c = \dot{m}_c c_p \left(T_{2,c} - T_{1,c} \right) \tag{3.8}$$

The bulk outlet temperatures $T_{2,e}$ and $T_{2,c}$ are determined as mentioned in section 3.3.1, by averaging the 15 values given

by each thermocouple grid. The reservoir power is defined as
the difference between the condenser and evaporator heat
transfer rates :

$$Q_R = Q_c - Q_e \qquad\qquad (3.9)$$

Effectiveness

The _effectiveness_ of a heat exchanger is a dimension-
less parameter used to compare the performance of different
heat exchangers or of the same heat exchanger under different
operating conditions. This quantity, denoted ε, is defined
as the ratio of the actual heat transfer rate in the heat
exchanger to the maximum thermodynamically possible heat
transfer rate. The maximum possible heat transfer rate is given
by the maximum temperature difference existing within the heat
exchanger, the difference between the two inlet temperatures,
times the lower value of the heat capacity rate of the flow :

$$Q_{max} = \left(\dot{m}c_p\right)_{min} \left[T_{1,e} - T_{1,c}\right]$$

In the present case, the heat capacity c_p of the air is
assumed constant; thus, $(\dot{m}c_p)_{min}$ always pertains to the flow
with the minimum mass flow rate.

The two principal heat transfer rates in the heat
exchanger, Q_e and Q_c, lead to two different definitions of
the effectiveness :

Evaporator effectiveness $\qquad \varepsilon_e = \dfrac{Q_e}{Q_{max}}$

Condenser effectiveness $\qquad \varepsilon_c = \dfrac{Q_c}{Q_{max}}$

There are two dimensionless parameters computed during the data reduction process which are useful both in prescribing the test conditions and organizing the effectiveness data. There are the mass flow ratio and the normalized reservoir temperature.

Mass flow ratio, MR

The mass flow ratio is defined as the air mass flow rate through the condenser section divided by the air mass flow rate through the evaporator :

$$MR = \frac{\dot{m}_c}{\dot{m}_e}$$

Normalized reservoir temperature, T_n

Since the reltionship of reservoir temperature to effectiveness is of primary interest in this study, it is necessary to express reservoir temperature in some way that permits comparisons of tests under different thermal loads for various reservoir temperatures. In order that the chosen transformation be valid, it must be independent of the performance of the heat exchanger, i.e., it must be independent of all temperatures downstream of the inlets. This leaves little choice but to define a parameter that indicates the reservoir temperature's relative position between the cold and hot air inlet temperatures :

$$T_n = \frac{T_R - T_{1,c}}{T_{1,e} - T_{1,c}}$$

It should be mentioned here that the liquid reservoir VCHP heat exchanger could be considered a reservoir power modulated system rather than a reservoir temperature modulated

one, in which case it would be appropriate to define a normalized reservoir power, Q_R/Q_{max}. A somewhat different test facility would have been required to conduct measurements from this point of view, one in which reservoir power could be accurately measured (now it can only be determined by taking the difference between Q_c and Q_e, which already are of only marginal accuracy). The author feels that the temperature formulation is more fundamental to the physical processes responsible for the variable conductance.

3.4.2 Global heat exchanger performance - Tests in large oil bath

A test matrix was established in which each point was defined by three main parameters : heater power, mass flow ratio and reservoir temperature. The heat exchanger was tested at thermal loads corresponding to heater settings of 2, 4 and 6 kW : at mass flow ratios of .4, .6, .8, and 1.0; and at irregular intervals in the normalized temperature range $0 < T_n < 1$. In addition, several tests were run at $T_n < 0$ and $T_n > 1$ to see the effect of operating outside the normal reservoir temperature range.

For each test point, the data acquisition system was activated once the test conditions (valve, air heater and rheostat settings) were established. The program output (heat transfer rates, effectiveness and temperature profile) was monitored until steady state was reached, typically taking about 20 minutes; then the DAS was stopped and reactivated, with subsequent acquisitions being recorded on magnetic cassette. An example af the DAS output appears in Appendix B.

The evaporator and condenser effectiveness for MR = 1 are plotted in figure 14. The points, although corresponding to tests under different thermal loads, admit of a relatively smooth curve fit, which validates the method of non-dimensionalizating the reservoir temperature. The two curves, evaporator

and condser effectiveness, cross at a point designated the ·
adiabatic operating point. At normalized reservoir tempera-
tures below the adiabatic operating temperature, the evaporater
effectiveness is higher than the condenser effectiveness, the
difference corresponding to the rate of heat transfer from the
heat pipes to the reservoirs. Under steady state conditions,
this heat loss can only be by conduction, since if it were by
convection the heat pipe wick would gradually empty of liquid.
This corresponds to a condition in which there is dryout at the
lower end of the evaporator section in at least some of the heat
pipes, a condition manifested by a steep gradient in the air tem-
perature profile measured at the exit of the evaporator section
(Fig. 15). The temperature profile shown probably represents
a superposition of several staggered temperature steps, since
the dryout boundary (if any) may be at a different location in
each row of heat pipes.

At the adiabatic operating point, there must be no
influx of liquid into the reservoir, since that would neces-
sitate reservoir heating in order to revaporize the fallen
liquid. There are, then, two possible adiabatic operating
situations : One is where the reservoirs are completely dried
out, with all of the liquid circulating in the heat pipes.
In this case, heat input to the reservoir serves only to main-
tain it at an elevated temperature (near the hot air inlet
temperature), compensating for heat losses by conduction
radiation, etc. The second is where there is some condenser
liquid in the reservoir; the adiabatic operating temperature
in this case is that at which the reservoir liquid is in
equilibrium with the heat pipe vapour. This situation is
plausible with or without dryout in the heat pipe evaporator
section.

Above the adiabatic operating point, the condenser
heat transfer is greater than that of the evaporator, being the
sum of the heat input to the evaporator and the heat input to
the reservoirs. The true effectiveness of the heat exchanger,
at any given operating temperature, must be regarded as the

lower of these two curves, since it is always the lower curve that represents the heat acutally exchanged between the two air streams, not taking into account heat which might have been lost or gained from the reservoirs. The significant feature of the super-adiabatic operating range ($T_n > T_a$) is that after increasing nearly linearly with T_n, the evaporator effectiveness reaches a peak and then decreases as the normalized reservoir temperature approaches 1.0. This decline in evaporator effectiveness is explained by the fact that at high normalized reservoir temperatures there is a low thermal gradient across the liquid layer in the evaporator section, and hence a low heat flux. The maximum in the evaporator effectiveness curve indicates the maximum heat exchange rate between air streams that can be achieved by the heat exchanger for these inlet conditions (and with uniform reservoir temperature).

The usable heat flux range can effectively be extended if one's principal purpose is to heat cold air. Although the maximum heat recovery from the hot air is given by the evaporator effectiveness, the heat supplied to the reservoirs is also recovered at the condensor; thus, in cases where the thermal potential of the evaporator is insufficient to meet the heat demand at the condenser, power can be supplied to meet the deficit. It should be noted, however, that this is an inefficient mode of operation, since increasing the normalized reservoir temperature beyond T_{max} reduces the effectiveness of the evaporator, so the additional reservoir power required to attain the desired rate of heat transfer at the condenser will be greater than the original deficit.

Figure 16 is a plot of the true heat exchanger effectiveness versus normalized reservoir temperature. It represents the ensemble of the large oil bath test results; all thermal loads and mass flow ratios are included. The effect of decreasing the ratio of mass flow rates from 1.0 is to displace the effectiveness curve upward and slightly to the right, giving both a higher maximum effectiveness and

higher optimal operating temperature. The rise in effectiveness
with decreasing mass flow ratio is typical of all fluid-to-
fluid heat exchangers.

3.4.3 Adiabatic operating point - Individually insulated reservoirs

For these tests each reservoir was wrapped in a
tightly fitting sleeve made of closed-cell foam. This indepen-
dent insulation allowed each row of heat pipes to establish its
own adiabatic operating regime. Indeed, it was found during
these tests that each heat pipe row had a slightly different
adiabatic operating temperature. To compare the results
obtained under these adiabatic test conditions with the "adia-
batic points" given by the intersection of the evaporator and
condenser effectiveness curves, one must average the tempera-
tures of the insulated reservoirs in order to obtain an
equivalent normalized reservoir temperature. The comparison
is therefore not rigrous, and some data suggests that it may
be misleading in the case where the heat transfer rate is a
small fraction of the heat exchanger's rated capacity. The
point corresponding to the highest heat transfer rate tested
(MR = 1, air heater power = 6 kw) is plotted against the
general effectiveness curves in figure 14.

An unexpected and still unexplained finding made
during the tests with individually insulated reservoirs is
that the first and third reservoirs had a higher temperature
than the second and fourth, the first row being the one closest
to the hot air inlet. One would expect the reservoir tempera-
tures to either increase or decrease monotonically from one
row to the next, depending on the direction of the flow. That
this is not the case indicates that for some reason the heat
pipe rows are not all operating in the same regime, as charac-
terized by their respective normalized reservoir temperature
evaluated with respect to the local evaporator and condensor
temperatures.

The results of these tests are summarized in table 1.
It is worth noting that the heat losses associated with adia-
batic operation increase, as a percentage of condenser effec-
tiveness, as the overall heat transfer rate decreases. This
is seen in the relatively large spread between the evaporator
and condenser effectiveness found in the last five rows of the
table.

3.4.4 Performance of a single row of heat pipes - Individual reservoir baths

To compare the individual performance of each row
of heat pipes, four tall narrow baths were used for reservoir
temperature control, three of them containing ice water and
the fourth containing oil with a resistance heater. The reser-
voirs were tested consecutively under the following (nominal)
conditions : MR = .8, heater power = 4 kW, normalized reservoir
temperature = 0.7.

The test results are summarized in table 2. They
show that there are no large-order differences in effectiveness
among the four rows of heat pipes. It is not clear whether the
differences that do exist result from differences in heat flux
path length in the fins, which varies with the position of the
heat pipe row tested, or rather differences in the heat pipes
themselves, such as non-uniformities in wick porosity, quantity
of working fluid, or in other basic heat pipe characteristics.
This question could be resolved with a numerical model of the
heat exchanger, capable of simulating single row operation.

4. DEVELOPMENT OF A NUMERICAL MODEL
OF THE HEAT EXCHANGER

4.1 Simplifying assumptions

In addition to the experimental investigation described above, it was undertaken to numerically model the heat exchanger. This represented a substantial challenge, for if the detailed behaviour of a single liquid reservoir VCHP is not fully understood, the overall comportment of a finned tube heat exchanger containing sixteen such heat pipes in cross-flow is understood still less. Having no prior indications as to the feasibility or validity of a complete computer model of the heat exchanger, we[*] considered it appropriate to begin with the following simplifying assumptions :

(1) There is no longitudinal temperature gradient in either the evaporator or condenser sections of the heat exchanger. Similarly, there are no transverse temperature gradients. The only non-uniform temperature profiles, whether of the fins or of the air, are in the flow direction.

(2) As in the experimental study, only steady state operation is considered.

(3) The liquid and vapour phases in the reservoirs are in equilibrium.

Consequently, there is no mass interchange between the heat pipes and the reservoirs. This condition corresponds to the adiabatic operation described in sections 3.4.2 and 3.4.3.

---

[*] This program was developed in conjunction with Paul-Hervé Theunissen, doctoral candidate at the Université Libre de Bruxelles.

4.2 Representation of the fin/tube system

As a consequence of assumption 1 of the preceeding section we may effectively compress all of the fins in the evaporator section into a single flat plate, and likewise those in the condenser section. Because the fins are thin and have high thermal conductivity, the plate temperature is assumed to be constant across its thickness. These two plates, one representing the evaporator side of the heat exchanger, the other the condenser side, are coupled to each other by the four rows of heat pipes. To facilitate an analytical (and therefore more elegant and efficient) solution of the air and fin temperature profiles, this coupling is simulated as a series of four linear heat sinks/sources normal to the flow direction, their position corresponding to that of the heat pipe rows. These four linear heat sinks and sources subdivide the evaporator and condenser plates, respectively, each into five "platelets" (Fig. 17), for which an analytical solution to the convective and conductive heat transfer equations can be developed.

Because of the high thermal conductivity of the fins and their large surface area relative to the heat pipe area, we assume that all of the heat transferred between the air and the heat pipes passes through the fins. In reality, the isothermal lines in the fins (plates) would tend to form contours around the heat pipes; due to the linearization of the heat sinks/sources, however, we make the further idealization that the isothermal lines are linear and perpendicular to the flow direction (in accordance with assumption 1 of the proceeding section).

4.2.1 The plate equations

In any given platelet, the two governing heat transfer equations are the one dimensional conduction equation,

$$ke \frac{d^2T}{dx^2} + h(T_a - T) = 0 \tag{4.1a}$$

and the convective heat transfer equation,

$$\frac{\dot{m}c_p}{w} \frac{dT_a}{dx} + h(T_a - T) = 0 \tag{4.2a}$$

where k = thermal conductivity of plate

e = plate thickness = (thickness of fin) ×
(number of fins)

h = total convective heat transfer coefficient =
(convective heat transfer coefficient) ×
(number of fin sides)

w = width of plate

$\dot{m}$ = total mass flow rate through one side of heat
exchanger

T = local plate temperature

T_a = local bulk air temperature

These equations can be simplified using the following non-dimensionalizations :

$$x = \frac{wh}{\dot{m}c_p}$$

$$\alpha = \frac{(\dot{m}c_p)^2}{w^2 ehk} \qquad \text{giving}$$

$$\frac{d^2T}{dx^2} + \alpha(T_a - T) = 0 \tag{4.1b}$$

$$\frac{dT_a}{dx} + T_a - T = 0 \tag{4.2b}$$

4.2.2 Solution for the plate temperature, T

Consider figure 18, which represents the ith
platelet.

Let $T_0 = T_i(0)$

$\quad\quad T_1 = T(X_i)$

$\quad\quad T_{a0} = \left. \left(T_a\right)_i^1 \right|_{\chi=0}$

$\quad\quad T_{a1} = \left. \left(T_a\right)_i \right|_{\chi=X_i}$

Integrating equation 4.1b once, after substituting the term
(T_a-T), one obtains

$$\frac{dT}{dX} - \left.\frac{dT}{\chi}\right|_0 = \alpha(T_a - T_{ao})$$

or

$$\frac{1}{\alpha}\frac{dT}{dX} + \left(T_{a0} - \left.\frac{1}{\alpha}\frac{dT}{dX}\right|_0\right) = T_a$$

Define $\quad T_\alpha \equiv \left(T_{a0} - \left.\frac{1}{\alpha}\frac{dT}{\chi}\right|_0\right)$; then $\qquad\qquad$ (4.3)

$$\frac{1}{\alpha}\frac{dT}{d\lambda} + T_\alpha = T_\alpha$$

Substituting back into equation (4.2b), one gets

$$\frac{d^2 T}{d\chi^2} + \frac{dT}{d\chi} - \alpha T + \alpha T_\alpha = 0$$

or

$$\frac{d^2(T-T_\alpha)}{d\chi^2} + \frac{d(T-T_\alpha)}{d\chi} - \alpha(T-T_\alpha) = 0$$

Equation 4.4 is a second order linear differential equation with the characteristic equation

$$r^2 + r - \alpha = 0$$

The general solution of this equation is

$$T-T_\alpha = Ae^{\omega_1 X} + Be^{\omega_2 X}$$

$$\text{where } \left.\begin{array}{c} \omega_1 \\ \\ \omega_2 \end{array}\right\} = \frac{-1 \pm \sqrt{1+4\alpha}}{2} \qquad (4.6ab)$$

4.2.3 Determination of constants A and B

We start with the implicit boundary conditions on T_0 and T_1 :

$$T_0 - T_\alpha = A+B$$

$$T_1 - T_\alpha = Ae^{\omega_1 X} + Be^{\omega_2 X}$$

Then,

$$A = (T_0 - T_\alpha) - B$$

Define $\Delta \equiv T - T_\alpha$. Then,

$$\Delta_1 = [\Delta_0 - B] e^{\omega_1 X} + B e^{\omega_2 X}$$

$$\therefore \quad B = \frac{\Delta_1 - \Delta_0 e^{\omega_1 X}}{e^{\omega_2 X} - e^{\omega_1 X}} \tag{4.7a}$$

$$A = \frac{\Delta_1 - \Delta_0 e^{\omega_2 X}}{e^{\omega_1 X} - e^{\omega_2 X}} \tag{4.7b}$$

The complete solution of the temperature profile for any given platelet is thus determined if T_0, T_1 and T_α are known. To determine T_α, $\left.\dfrac{dT}{dx}\right|_{x=0}$ must be determined in terms of the known temperatures, assumed for the moment to be T_0, T_1 and $T_{\alpha 0}$. Defferentiating equation 4.5 gives, at the platelet's leading edge :

$$\left.\frac{dT}{dx}\right|_{x=0} = \omega_1 A = \omega_2 B \tag{4.8}$$

$$\left.\frac{dT}{dx}\right|_{x=0} = \frac{\omega_1 (-\Delta_1 + \Delta_0 e^{\omega_2 X}) + \omega_2 (\Delta_1 - \Delta_0 e^{\omega_1 X})}{e^{\omega_2 X} - e^{\omega_1 X}}$$

Define $\beta_1 \equiv \dfrac{\omega_2 - \omega_1}{\left(e^{\omega_2 X} - e^{\omega_1 X}\right)}$ and $\beta_2 \equiv \dfrac{\left(\omega_1 e^{\omega_2 X} - \omega_2 e^{\omega_1 X}\right)}{\left(e^{\omega_2 X} - e^{\omega_1 X}\right)}$ (4.9ab)

then

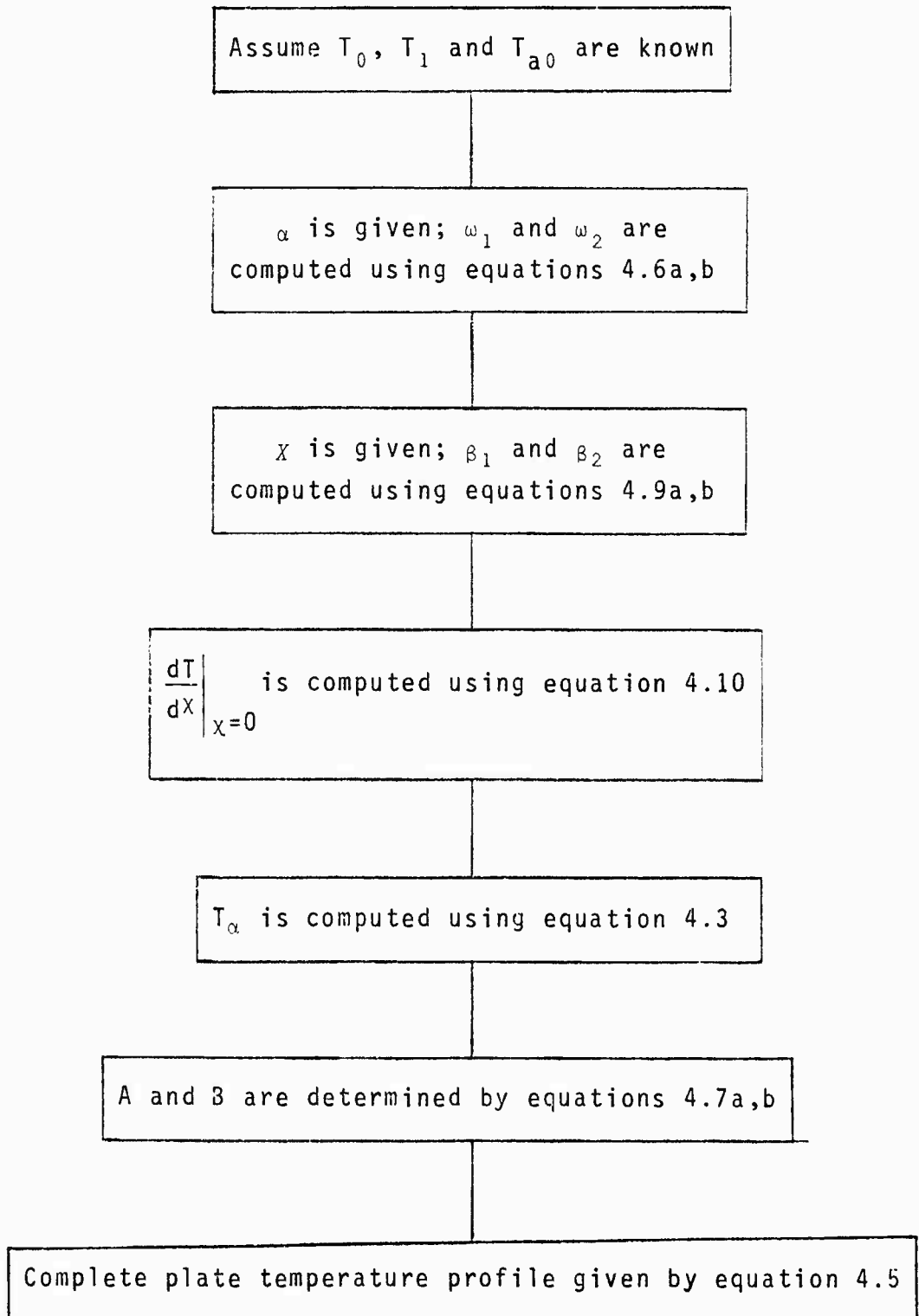$$\left.\frac{dT}{dx}\right|_{x=0} = \Delta_1 \beta_1 + \Delta_0 \beta_2$$

If one defines $\tilde{\Delta}_1 \equiv T_1 - T_{a0}$ and $\tilde{\Delta}_0 \equiv T_0 - T_{a0}$, it can be shown that

$$\left.\frac{dT}{dx}\right|_{x=0} = \frac{\tilde{\Delta}_1 \beta_1 + \tilde{\Delta}_0 \beta_2}{1 - \dfrac{1}{\alpha}(\beta_1 + \beta_2)} \tag{4.10}$$

Thus, $\left.\dfrac{dT}{dx}\right|_{x=0}$ hence $T\alpha$, has been determined in terms of the

"known" temperatures T_0, T_1 and T_{a0}, thereby enabling a complete solution of the platelet temperature profile.

4.2.4 Summary of platelet temperature calculation

$$\boxed{\text{Assume } T_0, \ T_1 \text{ and } T_{a0} \text{ are known}}$$

$$\boxed{\begin{array}{c}\alpha \text{ is given; } \omega_1 \text{ and } \omega_2 \text{ are} \\ \text{computed using equations 4.6a,b}\end{array}}$$

$$\boxed{\begin{array}{c}\chi \text{ is given; } \beta_1 \text{ and } \beta_2 \text{ are} \\ \text{computed using equations 4.9a,b}\end{array}}$$

$$\boxed{\left.\frac{dT}{dX}\right|_{\chi=0} \text{ is computed using equation 4.10}}$$

$$\boxed{T_\alpha \text{ is computed using equation 4.3}}$$

$$\boxed{A \text{ and } B \text{ are determined by equations 4.7a,b}}$$

$$\boxed{\text{Complete plate temperature profile given by equation 4.5}}$$

4.2.5 Solution for the air temperature, T_a

The expression for the air temperature is built up from equations 4.2b and 4.5.

$$\frac{dT_a}{dX} + T_a = T_\alpha + Ae^{\omega_1 X} + Be^{\omega_2 X} \tag{4.11}$$

The general solution to this differential equation is of the form

$$T_a = T_\alpha + Ce^{-X} + \xi_1 e^{\omega_1 X} + \xi_2 e^{\omega_2 X} \tag{4.12}$$

The particular solution is obtained as follows :

$$(\xi_1 + w_1\xi_1)e^{\omega_1 X} + (\xi_2 + \omega_2\xi_2)e^{\omega_2 X} = Ae^{\omega_1 \omega} + Be^{\omega_2 X}$$

$$\therefore \quad \beta_1 = \frac{A}{1-\omega_1} \qquad \xi_2 = \frac{B}{1+\omega_2}$$

The constant C is determined by setting X equal to zero :

$$T_{a0} - T_\alpha = C + \xi_1 + \xi_2$$

$$C = T_{a0} - T_\alpha - \xi_1 - \xi_2$$

$$C = \frac{1}{\alpha}\frac{dT}{dX}\bigg|_0 - \xi_1 - \xi_2$$

The air temperature at the platelet's trailing edge is then given as

$$Ta_1 = T_\alpha + Ce^{-X} + \xi_1 e^{\omega_1 X} + \xi_2 e^{\omega_2 X} \tag{4.13}$$

4.2.6 The temperature gradient in the platelet at the trailing edge

Equation 4.10 expresses the temperature gradient (which is proportional to the heat flux) in the platelet at its leading edge. A similar expression can be obtained for the trailing edge.

$$\left.\frac{dT}{dX}\right|_X = \omega_1 A e^{\omega_1 X} + \omega_2 B e^{\omega_2 X}$$

$$= \frac{\omega_1 \rho^{\omega_1 X}\left[-\Delta_1 + \Delta_0 e^{\omega_2 X}\right] + \omega_2 e^{\omega_2 X}\left[\Delta_1 - \Delta_0^{\omega_1 X}\right]}{\left(e^{\omega_2 X} - e^{\omega_1 X}\right)}$$

Define $S_1 \equiv \dfrac{-\omega_1 e^{\omega_1 X} + \omega_2 e^{\omega_2 X}}{e^{\omega_2 X} - e^{\omega_1 X}}$

$$S_2 \equiv \frac{(\omega_1 - \omega_2)e^{(\omega_1 + \omega_2)X}}{(e^{\omega_2 X} - e^{\omega_1 X})}$$

Then

$$\left.\frac{dT}{dX}\right|_{\ddot{X}} = \Delta_1 S_1 + \Delta_0 S_2 \tag{4.14}$$

4.2.7 Linearization of the equations

Equations 4.10, 4.13 and 4.14 are all implicitly linear equations in terms of the three temperatures, T_0, T_1, and T_{a0}, which up to now have been treated as known boundary conditions. The explicit expression of $\left.\frac{dT}{d\chi}\right|_0$, $\left.\frac{dT}{d\chi}\right|_\chi$ and T_{α_1}

in terms of these three variable involves length algebraic manipulations that will not be shown here. The resulting equations are given below :

(a) $\left.\dfrac{dT}{d\chi}\right|_0 = \gamma_1 T_1 + \gamma_2 T_0 - (\gamma_1 + \gamma_2) T_{a0}$ (4.15)

$$\text{where } \gamma_1 \equiv \frac{\beta_1}{1 - \dfrac{1}{\alpha}(\beta_1 + \beta_2)}$$

$$\gamma_2 \equiv \frac{\beta_2}{1 - \dfrac{1}{\alpha}(\beta_1 + \beta_2)}$$

(b) $\left.\dfrac{dT}{d\chi}\right|_\chi = \mu_1 T_1 - \mu_2 T_0 - (\mu_1 + \mu_2) T_{a0}$ (4.16)

$$\mu_1 = S_1 + \frac{(S_1 + S_2)\gamma_1}{\alpha}$$

$$\mu_2 = S_2 + \frac{(S_1 + S_2)\gamma_2}{\alpha}$$

(c) $\quad T_{a_1} = \nu_1 T_1 + \nu_2 T_0 - (\nu_1 + \nu_2 - 1)T_{a_0}$ $\qquad$ (4:17)

$$\nu_1 = \varepsilon_3 - \varepsilon_1 + \gamma_1 \varepsilon_6$$

$$\nu_2 = \varepsilon_2 - \varepsilon_4 + \gamma_2 \varepsilon_6$$

$$\varepsilon_1 = \frac{-e^{-X} + e^{\omega_1 X}}{(1+\omega_1)(e^{\omega_2 X} - e^{\omega_1 X})}$$

$$\varepsilon_2 = e^{\omega_2 X} \varepsilon_1$$

$$\varepsilon_3 = \frac{(-e^{-X} + e^{\omega_2 X})}{(1+\omega_2)(e^{\omega_2 X} - e^{\omega_1 X})}$$

$$\varepsilon_4 = e^{\omega_1 X} \varepsilon_3$$

$$\varepsilon_5 = e^{-X} - 1$$

$$\varepsilon_6 = \frac{\varepsilon_2 + \varepsilon_3 + \varepsilon_5 - \varepsilon_1 - \varepsilon_4}{\alpha}$$

4.2.8 Assembly of the platelets

Up to now, the entire analytical development has been with regard to a single platelet, a segment of the composite plate which represents one side of the heat exchanger. These segments, or platelets, are joined by lines of heat addition or removal, which represent the rows of heat pipes. For each side of the heat exchanger, our mathematical model links the platelets together using the physically imposed boundary conditions of continuity of temperature in the air and conservation

of energy in the platelet. At each node (boundary between platelets), the following conditions apply :

$$T_{a_0}^{i+1} = T_{a_1}^{i} \qquad (4.18)$$

$$\phi_i = kwe \left[\frac{dT}{dX}\bigg|_{X_i}^{i} - \frac{dT}{dX}\bigg|_{0}^{i+1} \right] \qquad (4.19)$$

where ϕ_i = heat addition rate at the boundary between platelets
i and i+1 (heat transfer rate in the ith row of the
pipes)

The boundary conditions at the entry and exit of the heat exchanger are the following:

(1) At the leading edge, the plate temperature is equal to the air temperature. This temperature is <u>not</u> the upstream inlet temperature of the air; due to stagnation effects at the leading edge of the fins, the air is preheated or precooled before actaully passing the $X_0 = 0$ line.

(2) At the trailing edge, it is assumed that there is no longitudinal temperature gradient (no heat conduction) in the fin. The exit air temperature is given by an equation of the type 4-17.

The above-stated conditions lead to a system of twelve equations in twelve unknowns for each side of the heat exchanger. Referring to figure 17, the equations for the top plate (condenser section) are as follows :

$$\text{Letting } \Phi = \frac{\phi}{kwe}$$

entry
$$\begin{bmatrix} T_0^o = T_{a0}^o \end{bmatrix} \tag{4.20}$$
$$T_{a_0}^o = T_{a\infty} + \frac{1}{\alpha} \left[\frac{dT}{d\chi}\right]_0^0 \tag{4.21}$$

row 1
$$\Phi_1 = \left[\frac{dT}{d\chi}\right]_{X_0}^0 - \left[\frac{dT}{d\chi}\right]_0^1 \tag{4.22}$$
$$T_{a0}^1 = T_a^0 \tag{4.23}$$

row 2
$$\Phi_2 = \left[\frac{dT}{d\chi}\right]_{X_1}^1 - \left[\frac{dT}{d\chi}\right]_0^2 \tag{4.24}$$
$$T_{a0}^2 = T_a^1 \tag{4.25}$$

row 3
$$\Phi_3 \quad \left[\frac{dT}{d\chi}\right]_{X_2}^2 - \left[\frac{dT}{d\chi}\right]_0^3 \tag{4.26}$$
$$T_{a0}^3 = T_{a_1}^2 \tag{4.27}$$

row 4
$$\Phi_4 = \left[\frac{dT}{d\chi}\right]_{X_3}^3 - \left[\frac{dT}{d\chi}\right]_0^4 \tag{4.28}$$
$$T_{a_0}^4 = T_a^3 \tag{4.29}$$

exit
$$\left[\frac{dT}{d\chi}\right]_{X_4}^4 = 0 \tag{4.30}$$
$$T_{a_1}^4 = \left[\nu_1 T_1 + \nu_2 T_0 - (\nu_1 + \nu_2 - 1)T_{a_0}\right]_{i=4} \tag{4.31}$$

A similar set of equations is obtained for the lower plate.
To solve this system of equations a matrix is composed of the
coefficients γ, μ, and ν given in section 4.9. The matrix
equation takes the form shown in figure 19, non-zero elements
indicated by squares and is given in tensorial notation by

$$\underline{\underline{A}} \cdot \underline{x} = \underline{B} T^{\circ}_{a0} + \underline{C}\alpha$$

We have, then, a system of equations in which the only
appearing unknowns, the vector $\underline{x}$, are the air and fin tempera-
tures at each discontinuity in the plate, precisely the values
needed to couple, by means of a mathematical model of the heat
pipes (to be described in the next section), the two sides of
the heat exchangers.

4.3 Numerical simulation of the heat pipes

Ideally, it would have been desirable to develop a
complete numerical model of the variable conductance heat pipe,
capable of representing its operation in all possible regimes,
thereby permitting a complete comparison with the experimental
results. Due to the complexity of the internal heat pipe phe-
nomena, however, such a model was beyond the scope of this
preliminary study. Instead, we limited ourselves to a model
of the heat pipe in its adiabatic reservoir regime, i.e., the
point at which heat is exchanged only between the evaporator and
condenser sections. This approach is justified, moreover, by
the fact that we have been until now unable to obtain much of
the information on the physical parameters of the heat pipe
construction (eg. wick thickness, wick porosity, effective pore
radius, wick material, etc) necessary to an accurate prediction
of its performance. Thus, even restricting ourselves to the
adiabatic operation of the heat pipes, we could only hope to
achieve qualitative agreement with the experimental results by
making appropriate guesses at the unknown parameters.

Our model is based on the simultaneous resolution of the equations expressing the relevant thermodynamic and hydrodynamic phenomena in the heat pipe. To attack the problem, it was first necessary to have a geometrical description of the liquid layer in the wick. On the basis of a survey of the longitudinal temperature distributions we measured under adiabatic operating conditions, a number of different idealized liquid profiles seemed plausible (see Fig. 20). Number 3 is the only one compatible with the assumption of constant heat flux over the entire evaporator section and over the entire condenser section, a condition necessary to the incorporation of this model into the finned tube model described in section 4.1. What follows is the development of heat and mass transfer equations for the model based on profile

4.3.1 Primary and secondary unknowns

These equations are formulated in terms of three primary unknowns and three secondary unknowns. The primary unknowns are

x_1 thickness of the liquid layer in the condenser wick

x_2 thickness of the liquid layer in the evaporator wick

x_3 working fluid mass flow rate through the adiabatic zone, $(\dot{m})_{max}$

The secondary unknowns are the temperatures on which the various fluid properties such as density and viscosity are dependent.

T_v vapour temperature

$\left(T_\ell\right)_e$ average temperature of the liquid in the evaporator

$\left(T_\ell\right)_c$ average temperature of the liquid in the condenser

4.3.2 Thermal resistance network

The heat transferred by the heat pipe must traverse a network of thermal resistances, which is represented in figure 21.

T_e temperature applied to the external surface of the evaporator

T_c temperature applied to the external surface of the condensor

T_v temperature of vapour in core of heat pipe (operating temperature)

RP_e thermal resistance across the heat pipe wall in the evaporator section

RW_e thermal resistance to conduction across the liquid layer in the evaporator section

RP_c thermal resistance across the heat pipe wall in the condensor section

R_c thermal resistance to axial conduction in the wall of the heat pipe

For a heat pipe in which there is not significant dry out the axial conduction in the walls is negligible with respect to the heat transfer by vapour transport, so R_c is neglected. Thus

$$Q = \dot{m}L = \frac{T_e - T_c}{RP_e + RW_e + RP_c + RW_c} \tag{4.32}$$

where the four resistances are given by

$$RP_e = \frac{\ell n(R_0/R_p)}{2\pi k_p \ell e}$$

$$RP_c = \frac{\ln(R_0/R_p)}{2\pi k_p \ell_c}$$

$$RW_e = \frac{\ln\left[R_p/(R_p - X_2)\right]}{2\pi k_w \ell_e}$$

$$RW_c = \frac{\ln\left[R_p/(R_p - X_1)\right]}{2\pi k_w \ell_c}$$

4.3.3 Pressure drop equilibrium in the heat pipe

Heat transfer in a heat pipe involves the working fluid in a cyclical process in which the fluid is pumped around a closed loop against certain pressure losses. During steady state operation, there must exist an equilibrium between the pumping forces and the drag forces on the working fluid. The pressure losses undergone by the fluid arise from the viscous resistance to the flow in both the wick and the vapour core, and from the momentum loss (or gain) of the vapour due to the mass transfer at the liquid/vapour interface.

The pumping forces are the capillary force on the liquid, which is due to the variation in the radius of curvature of the liquid menisci along the wick, and the body forces on the fluid, which are limited to the force of gravity in the present case. The weight of the vapour is very small compared to the weight of the liquid and is therefore neglected.

This equilibrium is expressed by the following equation, where pumping pressure gradients are assumed to be positive in the flow direction, and drag pressure gradients negative :

$$\Delta p_c + \Delta p_g + \Delta p_\ell + \Delta p_v = 0 \tag{4.33}$$

where Δp_c pressure difference due to capillary forces

Δp_g pressure difference due to gravity

Δp_ℓ pressure drop in liquid

Δp_v pressure drop in vapour

This equation can be written in integral form, with z defined as the direction of liquid flow :

$$\int_{z_1}^{z_2} \left[\frac{dp_c}{dZ} + \frac{dp_g}{dz} + \frac{dp_\ell}{dz} - \frac{dp_v}{dz} \right] \, dz = 0 \tag{4.34}$$

4.3.4 Pumping forces

Capillary liquid pressure gradient

In the case of a class B wick (in which the reduced capillary force is independent of the wetting angle of the liquid/solid interface, but is rather a function of pore geometry), the maximum capillary pressure gradient is given by

$$\frac{dp_c}{dz} = \frac{2\sigma}{r_p(\ell_e + \ell_a + \ell_c)}$$

where σ surface tension of liquid/vapour interface

r_p effective pore radius in the wick

Gravitational liquid pressure gradient

This term is simply the density of the liquid times the acceleration due to gravity :

$$\frac{dp_g}{dz} = \rho_\ell g$$

4.3.5 Drag forces

Viscous liquid pressure gradient

This term is given by a form of Darcy's law, adapted
for flow in porous media. It is usually used for fully satu-
tated wicks, with A denoting the full cross-sectional area of
the wick. In this case, however, A represents only the wetted
area and depends on the thickness of the liquid layer in the
wick. Cotter (Ref. 4) gives the following expression for the
liquid pressure gradient :

$$\frac{dp_\ell}{dz} = \frac{-\nu_\ell \; \dot{m}_\ell(z)}{K \; A(z)}$$

where $\dot{m}_\ell$ local liquid mass flow rate   (m/s)

   K   wick permeability   (m^2)

   A   local liquid flow area   (m^2)

Vapour pressure gradient

The vapour pressure gradient can be divided into
two distinct terms, one due to viscous shear and the other
due to mass transfer, indicated by

$$\left(\frac{dp_v}{dz}\right)_f \qquad \text{and} \qquad \left(\frac{dp_v}{dz}\right)_m$$

respectively. The expression for the viscous pressure loss
is similar to that for the liquid. The momentum pressure
gradient depends on the rate of mass addition (or removal) at
the wick boundary and thus contains the derivative of the mass
transfer rate with respect to position. Katsoff's (Ref. 5)
equations for each of these terms are

$$\left(\frac{dp_v}{dz}\right)_f = \frac{8 \, \nu_v \dot{m}(z)}{\pi R_v^4}$$

$$\left(\frac{dp_v}{dz}\right)_m = \frac{8\dot{m}(z)}{3\pi^2 \rho_v R_v^4} \frac{d\dot{m}(z)}{dz}$$

where R_v radius of vapour core

     ν_v kinematic viscosity of vapour

     ρ_v density of vapour

4.3.6 The heat pipe equations

The liquid profile in the wick chosen for this model imposes certain boundary conditions on the pressure balance equations. Since the thickness of the liquid layer is constant over the whole condenser section and the whole evaporator section, according to the resistance model the heat transfer rate also must be constant. This implies that in the pressure balance equations, $\frac{d\dot{m}}{dz}$ is constant over each section. Additionally, since there is no mass interchange with the reservoir, the mass flow rate is zero at both ends of the heat pipe.

Expanding equation 4.32, and integrating 4.34 over the length of the evaporator and over the length of the condenser, one obtains the following set of three non-linear algebraic equations in the primary and secondary unknowns introduced in section 4.21 :

$$f_1,(x_1,x_2,x_3) = 0 = \left[\frac{4}{3\pi^2 \ell_c \rho_v(T_v)R_v^4}\right] x_3^2 - \left[\frac{\nu_\ell(T_\ell)_c}{2KA_\ell(x_1)} + \frac{4\nu_v(T_v)}{\pi R_v^4}\right] x_3$$

$$+ \left[g_{\rho\ell}(T_\ell)_c + \frac{2\,\sigma\,(T_v)}{r_p(\ell_e+\ell_a+\ell_c)}\right] \qquad (4.35)$$

$$f_2(x_1,x_2,x_3) = 0 = \left[\frac{4}{3\pi^2 \ell_e \rho_v(T_v) R_v^4}\right] x_3^2 + \left[\frac{\nu_\ell(T_\ell)_e}{2KA_\ell(x_2)} + \right.$$

$$\left. + \frac{4\nu_v(T_v)}{\pi R_v^4}\right] x_3 - \left[g\rho_\ell(T_\ell)_e + \frac{2\sigma(T_v)}{r_p(\ell_e+\ell_a+\ell_c)}\right] \quad (4.36)$$

$$f_3(x_1,x_2,x_3) = 0 = x_3 L -$$

$$- \frac{T_e - T_c}{\left(\frac{1}{\ell_e} + \frac{1}{\ell_c}\right)\left[\frac{\ell n(R_0/R_p)}{2\pi k_p}\right] + \left(\frac{1}{2\pi k_w}\right)\left[\frac{\ell n[R_p/(R_p - x_2)]}{\ell_e} + \frac{\ell n[R_p/R_p - x_1)]}{\ell_c}\right]}$$
$$(4.37)$$

A complementary set of relations, based on the thermal resistance model resistance model of figure 21, is used to evaluate the secondary unknowns :

$$T_v = T_e - x_3 L(RP_e + RW_e) \quad (4.38)$$

$$(T_\ell)_e = T_v + \frac{1}{2} x_3 L(RW_e) \quad (4.39)$$

$$(T_\ell)_c = T_v - \frac{1}{2} x_3 L(RW_c) \quad (4.40)$$

4.3.7 Method of solution

In the FORTRAN program, equations 4.35 to 4.37 are
solved iteratively using Newton's method. The input to the
heat pipe subroutine consists of the known heat pipe proper-
ties and the external temperatures of the evaporator and
condenser sections. The output consists of the heat flux and
heat pipe operating temperature.

A matrix is constructed of the partial derivatives
of the three functions f_1, f_2 and f_3, defining a system of
linear independent equations which are then solved by Gaussian
elimination to yield a correction vector containing the in-
crements to be added to each of the primary unknowns in order
to improve the accuracy of the initial estimates. After each
iteration, the secondary unknowns are reevaluated using
equations 4.38 to 4.40, and the new values are used in deter-
mining the values of the fluid properties to be used in the
next iteration. This procedure is repeated until the desired
tolerances on the x values have been met.

The stability of this method seems to be very sen-
sitive to several of the physical heat pipe parameters, notably
the permeability and porosity of the wick. A damping factor
is currently used to retard convergence and thereby to avoid
accidental divergence from an actual solution.

4.4 Coupling the finned tube model
to the heat pipe model

The critical step in modelling the entire heat
exchanger is the incorporation of the heat pipe model into
the previously described solution of the finned tube system.
What follows is a brief explanation of the global solution
algorithm.

To start, an overall heat exchanger effectiveness of
50% is assumed, and the heat fluxes in all of the heat pipes
are assumed equal. This gives initial values for the heat
fluxes $\phi_{i=1,4}$ in vector $\underline{C}$ of the system of equations shown
in figure 19. The inlet air temperatures are given, so the
corresponding set of equations for both sides of the heat
exchanger can be solved, thereby giving the air and fin tempera-
tures at each node. These temperatures are computed on the
basis of an arbitrarily assumed heat flux which most probably
does not correspond to the actual performance of the heat pipes
at the specified air inlet conditions. When the heat pipe
subroutine is called, however, new values are provided for the
heat flux in each row of heat pipes. These new values replace
the previous ones in the vector $\underline{C}$ in the parallel systems of
equations (evaporator and condenser side), enabling one to
recompute the air and fin temperatures at each node. The pro-
cess is repeated until convergence is obtained.

The output values of particular interest are T_{a1}^4 for
each side of the heat exchanger, which correspond to TE(2) and
TC(2) in the terminology of the experiments. With these data,
the heat exchanger effectiveness is computed to facilitate
comparison with the experimental results. The operating tem-
perature of each row of heat pipes, passively determined in
the process of convergence, is included in the program's out-
put, as it is of interest in determining the operating regime
of the heat exchanger predicted by the program.

4.5 Computational results

Since we had almost no information on the internal
construction of the heat pipes, informed guesses had to be made
to provide the computer program with some of the necessary in-
put parameters, particularly those concerning the wick.
Although perhaps not the real configuration, the wick was assumed
to be of single annular geometry with isotropic and uniform

porosity. Several physical properties seem to play a major
role in determining the stability of the procedure, notably
the porosity (void fraction) and permeability of the wick.
The values of these parameters were chosen so as to obtain
convergence of the solution; they do lie, however, within the
range of physically reasonable values. A summary of the heat
exchanger parameters used in the computations appears in
Appendix C.

The program HPIPE was run for a variety of air flow
conditions matching those of the experiments. A sample of
the program output, with only the final iteration shown,
appears in Appendix D. The air and fin temperature is given
for each node (fin-tube intersection) as well as the vapour
temperature (reservoir temperature for each row of heat pipes.
A plotting routine was developed for the program, permitting
the visualization of the evaporator and condenser section air
and fin temperature profiles given by the numerical solution.
Figures 22-29 show the temperature profiles computed for the
various air inlet temperatures and mass flow ratios tested.
It is important to note the difference in nature between the
air and fin temperature profiles, whereas the air's tempera-
ture changes monotonically as it passes through the heat
exchanger, the fin temperature gradient often changes sign at
the heat pipe rows, indicating a heat flux either into
(evaporator) or out of (condenser) the heat pipes both upstream
and downstream of each row. The existence of these cusps in
the fin temperature profile depends on the relative magnitude
of the equivalent heat pipe thermal conductivity, the fin
thermal conductivity, and the coefficient of convection of the
air flows.

For the highest thermal load tested, corresponding to
an inlet temperature of 65°C, the four effectivenesses computed
for the four different mass flow ratios are in fairly good
agreement with the experimental curves when plotted versus
their respective average normalized reservoir (Fig. 30).

Thus, it seems that despite the large uncertainty associated with many of the heat pipe parameters, the numerical heat exchanger model does approximate the heat exchanger effectiveness in one particular operating regime. There is a major discrepancy, however, in that the reservoir temperature predicted by the program, which is based on the assumption of adiabatic reservoirs, are consistently higher than the experimentally determined adiabatic operating temperature for the same thermal load. This discrepancy can perhaps be corrected with a more detailed knowledge of the real heat pipe parameters. It is possible, however, that the assumption of a constant liquid profile in the wick of the evaporator and condenser sections is an oversimplification, inadequate to simulate the actual heat pipe behaviour, which may include significant dryout zones or non-linear liquid thickenss gradients.

To permit the numerical simulation of the heat exchanger over the entire normalized temperature operating range, as well as to improve the prediction of the adiabatic operating point, two modifications of HPIPE are currently being undertaken :

(1) The heat pipe simulation will be expanded to take into account an arbitrary heat input to the reservoir, hence a vapour flux from the reservoir to the heat pipe. For given air inlet conditions, the operating temperature and effectiveness of the heat exchanger will be functions of the reservoir input energy.

(2) Rather than treating the evaporator and condenser sections as single entities with constant liquid profiles, each section will be divided into finite elements, with the possibility of a different liquid thickness, heat transfer rate, and temperature boundary conditions for each element.

5. CONCLUSION

The research presented in this report confirms that the use of heat pipes permits the construction of compact and effective air-to-air heat exchangers. The liquid reservoir VCHT can be considered a sort of thermal transistor (evaporator = emitter, condenser = collector, reservoir = base) in which the primary heat flux between the evaporator and condenser is modulated by a secondary heat flux, the energy input to the reservoir. The normalized reservoir temperature, the mass flow ratio, and the effectiveness are three non-dimensionalizations which allow the coherent representation of heat exchanger performance over a wide range of operating conditions. The effectiveness data, when normalized in this way, lie on curves which exhibit two important properties :

(1) There exists a peak in the effectiveness curves which indicates both the maximum attainable heat flux and the operating temperature at which this maximum is reached.

(2) Below this temperature, there is a nearly linear variation of effectiveness over a broad temperature band, which would facilitate the design of a control system.

For control pupposes, the heat exchanger can be considered either reservoir temperature moduiated or reservoir power modulated. The power modulated concept is more direct, since temperature regulation is ultimately achieved by power modulation anyway.

The HPIPE program, once it has been modified to simulate complete variable conductance operation, will be a useful tool in the design of VCHP heat exchangers and in the development of a suitable control system. It appears that the structure of the program is both sound and efficient and that with the aid of more complete design information and a discretization of the heat exchanger along the length of the heat pipes as well as in the flow direction, a high degree of accuracy can be obtained.

REFERENCES

1. THEUNISSEN, P-H.: Système d'acquisition de données, SUN VKI

2. Listings of the mini-computer programs are held by Professor J-M. Buchlin, VKI.

3. HANSEN, K.: Measurements on a variable conductance heat pipe heat exchanger. VKI SR 1981-01/EA, May 1981.

4. MARCUS, B.D.: Theory and design of variable conductance heat pipes. NASA CR 2018, April 1972, p 8.

5. ibid. p. 11

APPENDIX A - HEAT EXCHANGER SPECIFICATIONS

N_p number of heat pipes :   16 (in a square 4 x 4 array)

      number of reservoirs :   4 (1 per row of heat pipes)

Materials

housing   : aluminum

fins   : aluminum

heat pipes   : copper

reservoirs   : reservoirs

wick   : ?

working fluid : methylchloride (Freon 40)

Dimensions

ℓ_e	evaporator length	:	.24 m
ℓ_c	condenser length	:	.22 m
ℓ_a	length of adiabatic zone :	:	.02 m
s	fin spacing	:	1.72 mm
w	width of heat exchanger	:	.13 m
	depth of heat exchanger (flow path length) :	:	.13 m
d_p	diameter of heat pipes	:	.013 m
	heat pipe spacing	:	.034 m
	diameter of reservoirs	:	.020 m

APPENDIX B - SAMPLE DATA ACQUISITION SYSTEM OUTPUT

```
DATE:7/5/81
TITLE:.8/6/65
CONFIGURATION COUNTER=1,PARALLEL=0:  1
CARACTERISTIQUES DES CHNNAUX A/D
------------------------------------
CANAL              1        THERM        56
CANAL              2        MEVAP         1
CANAL              3        MCOND         1
 CANAL          4           NON RACCORDE
 CANAL          5           NON RACCORDE
 CANAL          6           NON RACCORDE
 CANAL          7           NON RACCORDE
 CANAL          8           NON RACCORDE
----------------------------------------------------------------
 0            TEMPS: 0 SEC
TEMP  0-7   +   .0 +32.2 +32.0 +72.2 +72.8 +67.2 +  .0 +  .0
 TEMP 8-15  +58.3 +58.8 +58.8 +58.2 +59.2 +59.4 +58.4 +59.9
 TEMP 16-23 +52.3 +53.1 +52.8 +52.3 +51.3 +50.7 +50.7 +50.6
 TEMP 24-31 +  .0 +  .0 +  .0 +  .0 +  .0 +  .0 +  .0 +  .0
 TEMP 32-39 +  .0 +  .0 +  .0 +  .0 +  .0 +  .0 +  .0 +  .0
 TEMP 40-47 +59.1 +59.1 +60.0 +60.1 +58.9 +61.0 +60.8 +  .0
 TEMP 48-55 +50.4 +50.8 +49.8 +50.1 +51.6 +51.1 +50.8 +  .0
 PE:  8.086696 MM H2O  MEVAP:  .106228883 KG/SEC
 PC:  6.44871396 MM H2O  MCOND:  .0792523501  KG/SEC
 TRES:  67.2292988 'C       MASS FLOW RATIO:  .746052747
NORMALIZED RESERVOIR TEMPERATURE:  .86878022
 TE(1):  72.528554  TE(2):  59.3699916
 TC(1):  32.1439782  TC(2):  51.2921618
HEAT TRANSFER RATE:  QE= 1.40900195  KW    QC= 1.52967886  KW
POWER RATIO:  QE/QC=  .921109642
 EE:  .436740419    EX:  .474145963
NORMALIZED RESERVOIR HEAT TRANSFER:  QR/QE=  .0856470871   QR/QC=  .078890357
 LONGITUDINAL TEMPERATURE DISTRIBUTION
TL( 1 )=    60.2520775
TL( 2 )=    59.7690912
TL( 3 )=    59.1913034
TL( 4 )=    58.9864947
TL( 5 )=    58.6509912
TL( 6 )=    51.2399422
TL( 7 )=    50.290892
TL( 8 )=    50.6329261
TL( 9 )=    51.5049626
TL( 10 )=   52.7920862
```

```
----------------------------------------------------------------
 1              TEMPS: 109 SEC
TEMP  0-7    + .0 +31.9 +31.7 +72.0 +72.3 +66.7 +  .0 +  .0
 TEMP 8-15   +57.9 +58.4 +58.4 +57.7 +58.9 +59.1 +58.0 +59.4
 TEMP 16-23  +52.1 +52.7 +52.4 +51.9 +50.8 +50.4 +50.3 +50.5
 TEMP 24-31  +  .0 +  .0 +  .0 +  .0 +  .0 +  .0 +  .0 +  .0
 TEMP 32-39  +  .0 +  .0 +  .0 +  .0 +  .0 +  .0 +  .0 +  .0
 TEMP 40-47  +58.7 +58.6 +59.6 +59.8 +58.5 +60.5 +60.4 +  .0
 TEMP 48-55  +50.1 +50.5 +49.5 +49.8 +51.3 +50.7 +50.6 +  .0
 PE:  8.203104  MM H2O  MEVAP:  .100727553  KG/SEC
 PC:  6.72312732  MM H2O  MCOND:  .0816284496  KG/SEC
 TRES:  66.7894924 'C       MASS FLOW RATIO:  .81038849
NORMALIZED RESERVOIR TEMPERATURE:  .865862623
 TE(1):  72.2025873  TE(2):  58.982272
 TC(1):  31.8477284  TC(2):  50.9584425
HEAT TRANSFER RATE:  QE= 1.34230321  KW    QC= 1.57245778  KW
POWER RATIO:  QE/QC=  .853633864
 EE:  .404252502    EX:  .473566619
NORMALIZED RESERVOIR HEAT TRANSFER:  QR/QE=  .17146243   QR/QC=  .146366136
 LONGITUDINAL TEMPERATURE DISTRIBUTION
TL( 1 )=   59.8800687
TL( 2 )=   59.39658
TL( 3 )=   58.7437604
TL( 4 )=   58.6133442
TL( 5 )=   58.2776065
TL( 6 )=   50.9365081
TL( 7 )=   49.9868285
TL( 8 )=   50.3290574
TL( 9 )=   51.087948
TL( 10 )=   52.4518702


----------------------------------------------------------------
 2              TEMPS: 218 SEC
TEMP  0-7    + .0 +31.9 +31.8 +71.9 +72.5 +66.3 +  .0 +  .0
 TEMP 8-15   +58.1 +58.5 +58.6 +58.0 +59.1 +59.2 +58.2 +59.6
 TEMP 16-23  +52.2 +52.9 +52.7 +52.0 +51.1 +50.6 +50.4 +50.7
 TEMP 24-31  +  .0 +  .0 +  .0 +  .0 +  .0 +  .0 +  .0 +  .0
 TEMP 32-39  +  .0 +  .0 +  .0 +  .0 +  .0 +  .0 +  .0 +  .0
 TEMP 40-47  +58.9 +59.0 +59.9 +60.0 +58.9 +60.6 +60.5 +  .0
 TEMP 48-55  +50.3 +50.7 +49.8 +50.1 +51.5 +51.1 +50.7 +  .0
 PE:  8.6132592  MM H2O  MEVAP:  .10405466  KG/SEC
 PC:  6.72312732  MM H2O  MCOND:  .0816284496  KG/SEC
 TRES:  66.3492644 'C       MASS FLOW RATIO:  .784476633
NORMALIZED RESERVOIR TEMPERATURE:  .853590829
 TE(1):  72.2568525  TE(2):  59.1911218
 TC(1):  31.9070019  TC(2):  51.1709153
HEAT TRANSFER RATE:  QE= 1.37042657  KW    QC= 1.58506325  KW
POWER RATIO:  QE/QC=  .864587943
 EE:  .412773454    EX:  .477422173
NORMALIZED RESERVOIR HEAT TRANSFER:  QR/QE=  .15662034   QR/QC=  .135412058
 LONGITUDINAL TEMPERATURE DISTRIBUTION
TL( 1 )=   60.0663381
TL( 2 )=   59.6573855
TL( 3 )=   58.967586
TL( 4 )=   58.7999645
TL( 5 )=   58.464335
TL( 6 )=   51.1641022
TL( 7 )=   50.2529397
TL( 8 )=   50.5189858
TL( 9 )=   51.2776361
TL( 10 )=   52.6409129
```

APPENDIX C - <u>VALUES OF PARAMETERS USED IN THE</u> <u>HPIPE CALCULATIONS HEAT EXCHANGER</u>

Heat exchanger

length of evaporator   : .24 m
length of condenser   : .22 m
length of adiabatic zone : .02 m

Pipes

external heat pipe diameter : .013 m
internal heat pipe diameter : .011 m
vapour core diameter   : .009 m

Wick

wick thickness   : .001 m
porosity   15%
permeability $1. \times 10^{-9}$ m2
thermal conductivity of wick material : 100 W/m°C
effective pore radius   : .0005 m

Fins

fin spacing   .00172 m
fin thickness   .0005 m
thermal conductivity 384 W/m°C
length of platelets
    x_1 .014 m
    x_2, x_3, x_4 .034 m
    x_5 .014 m

Working fluid

liquid density :

$$\rho_{\ell}(T_{\ell}) = -(1.818\times10^{-4})T_{\ell}^{3}+(1.125\ 10^{-2})T_{\ell}-(2.128)T+960 \quad (kg/m^3)$$

$$[T_{\ell}] = \ ^{\circ}C$$

vapour density :

$$\rho_{V}(T_{V}) = (1.441\times10^{-4})T_{V}^{3}-(5.762\times10^{-3})T_{V}^{2}+(.2965)T_{V}+6.066 \quad (kg/m^3)$$

$$[T_{V}] = \ ^{\circ}C$$

liquid viscosity :

$$\mu_{1} = .6931\ T_{\ell}^{1.5}\ exp\left(\frac{331.9}{T_{\ell}}\right) \qquad Ns/m^2$$

$$[T_{\ell}] = \ ^{\circ}K$$

vapour viscosity :

$$\mu_{V} = (15.92\ 10^{-7})\ T_{V}^{0.5}/\ (1+462.1/T_{V}) \qquad Ns/m^2$$

$$[T_{\ell}] = \ ^{\circ}K$$

latent heat of vaporization :

$$4.2\times10^{5} \quad J/kg$$

thermal conductivity of liquid :

$$.07 \qquad W/m^{\circ}C$$

APPENDIX D - SAMPLE OUTPUT OF HPIPE

```
*********************************************************************************************
  PROPRIETE DU HEATPIPE
  RADP:.0055  RL:.07  RCU:385.  RADV:.0045
  RADF:.0005  EPS:.15  KW:100.  MAXIT:50  RELHP:.2
  LE:.24  LC:.22  LA:.02  RADO:.0065  KP:.4648228692852
  L:420000.  RPP:.00006905845661127  FWP:.3423994128542
  G(1-5):329450119.7817 3.183101550489E+9 3.104991605415E+9 9.807 8330.333333333
  DELTA(1-3):1.E-10 1.E-10 1.E-10  N:3
*********************************************************************************************
FIG.     AIR (A) AND FIN (F) TEMPERATURE PROFILES IN THE
         EVAPORATOR (E) AND CONDENSER (C) SECTIONS OF AN
                  HEAT PIPE HEAT EXCHANGER.
         (+) HEAT PIPE VAPOR TEMPERATURE
         AIR INLET TEMPERATURES 65 C, 30 C ; MASS FLOW RATIO 1.
TEMP (C)
    LENGTH (M)
 TMAX:80.  TMIN:20.  NY:6
 PROPRIETE DU CONDENSEUR
  MC:.75  TCI:30.  HC:42900.  LC:100.  EC:.065  CPC:1008.
  LGC:.014 .034 .034  034 .014
 PROPRIETE DE L'EVAPORATEUR
  ME:.75  TEI:65.  HE:46200  LE:100.  EE:.07  CPE:1008.
  LGE:.014 .034 .034 .034 .014
  COUNTER:T  MODECH.1
  XHP:30.
  EPS:.001  NLIM.50  REL:.4  IMPIT:F
*********************************************************************************************
  CONDENSEUR
AC:2.049618074203  STC:56 74503174503
XLC: 7944444444444 1.929365079365 1 929365079365 1.929365079365 .7944444444440
  EVAPORATEUR
  AE:1.767272727273  STE:61.111111111111
  XLE:.8555555555556 2.077777777778 2 077777777778 2 077777777770 .8555555555556
*********************************************************************************************
*********************************************************************************************
  ITERATION #8
  CONDENSEUR
TA:     42.19        41.24        39.40        35 40        32.48        31.60
T:      42.83        43.44        40 79        37 82        34 69        31.60
FL:                  .2310E+04    .2285E+04   2293E+04     .2330E+04
TV:                  52.15        49 27        46 29        43 40
T:      63.37        60.44        57 02        54 34        51 69        52 24
TA.     63.37        62 47        57 54        56.56        53 72        52 80
  EVAPORATEUR
*********************************************************************************************
  SOLUTION DU CONDENSEUR
  RACINE EQ CARACT. W1= .1016E+01  W2=- 2016E+01
*********************************************************************************************
```

* PLAQUETTE *	#	T1	EXP(W1*X)	EXP(W2*X)	EXP(-X)
	1	.3000E+02	.2137E+01	-.5433E+00	
	2	.3300E+02	.6644E+00	.9430E+00	
	3	.3611E+02	.4592E+00	.1053E+01	
	4	.3914E+02	.6039E+00	.1052E+01	
	5	.4219E+02	.1377E+00	.1062E+01	

AIR	#	TI	EXP(W1*X)	EXP(W2*X)	EXP(-X)
	1	.3000E+02	.1061E+01	.5347E+00	-.2842E-13
	2	.3308E+02	.3295E+00	-.9278E+00	-.4619E-13
	3	.3611E+02	.3250E+00	-.1036E+01	-.1421E-13
	4	.3914E+02	.2990E+00	-.1035E+01	-.3055E-12
	5	.4219E+02	.9390E-01	-.1045E+01	.2132E-13

SOLUTION DE L'EVAPORATEUR
RACINE EQ CARACT: W1= .9503E+00 W2=-.1920E+01

PLAQUETTE	#	TI	EXP(W1*X)	EXP(W2*X)	EXP(-X)
	1	.6500E+02	-.2116E+01	.4860E+00	
	2	.6174E+02	-.6795E+00	-.8141E+00	
	3	.5891E+02	-.6730E+00	-.9167E+00	
	4	.5588E+02	-.6170E+00	-.9214E+00	
	5	.5280E+02	-.1720E+00	-.9367E+00	

AIR	#	TI	EXP(W1*X)	EXP(W2*X)	EXP(-X)
	1	.6500E+02	-.1102E+01	-.5281E+00	.1776E-12
	2	.6194E+02	-.3538E+00	.8842E+00	-.1208E-12
	3	.5891E+02	-.3505E+00	.9961E+00	-.4476E-12
	4	.5588E+02	-.3210E+00	.1001E+01	-.3624E-12
	5	.5280E+02	-.8958E-01	.1018E+01	.1421E-13

EFFICACITE DE L'ECHANGEUR .487065511017

Mass flow ratio	Heater power	Normalized reservoir temperatures				ε_e	ε_c
		1	2	3	4		
1.	6 kW	.37	.33	.36	.32	.29	.30
.8	6	.37	.32	.39	.31	.31	.32
.6	6	.37	.32	.39	.30	.37	.36
.4	6	.36	.32	.40	.31	.41	.40
1.	4	.28	.22	.27	.20	.26	.25
.8	4	.32	.26	.32	.26	.30	.30
.6	4	.33	.27	.34	.28	.35	.34
.4	4	.31	.26	.33	.28	.42	.37
1.	2	.23	.12	.24.	.14	.22	.21
.8	2	.19	.10	.22	.11	.24	.22
.6	2	.16	.07	.18	.09	.27	.19
.4	2	.16	.06	.17	.12	.35	.24

TABLE 1 - SUMMARY OF TEST RESULTS WITH INDIVIDUALLY HEATED RESERVOIRS

Row	Mass flow ratio	T_n	ε_e	ε_c
1	.80	.70	.216	.206
2	.80	.70	.218	.224
3	.80	.70	.213	.218
4	.80	.70	.185	.216

Heater Power = 4 kW

TABLE 2 - SUMMARY OF THE TEST RESULT WITH INDIVIDUAL RESERVOIR BATHS
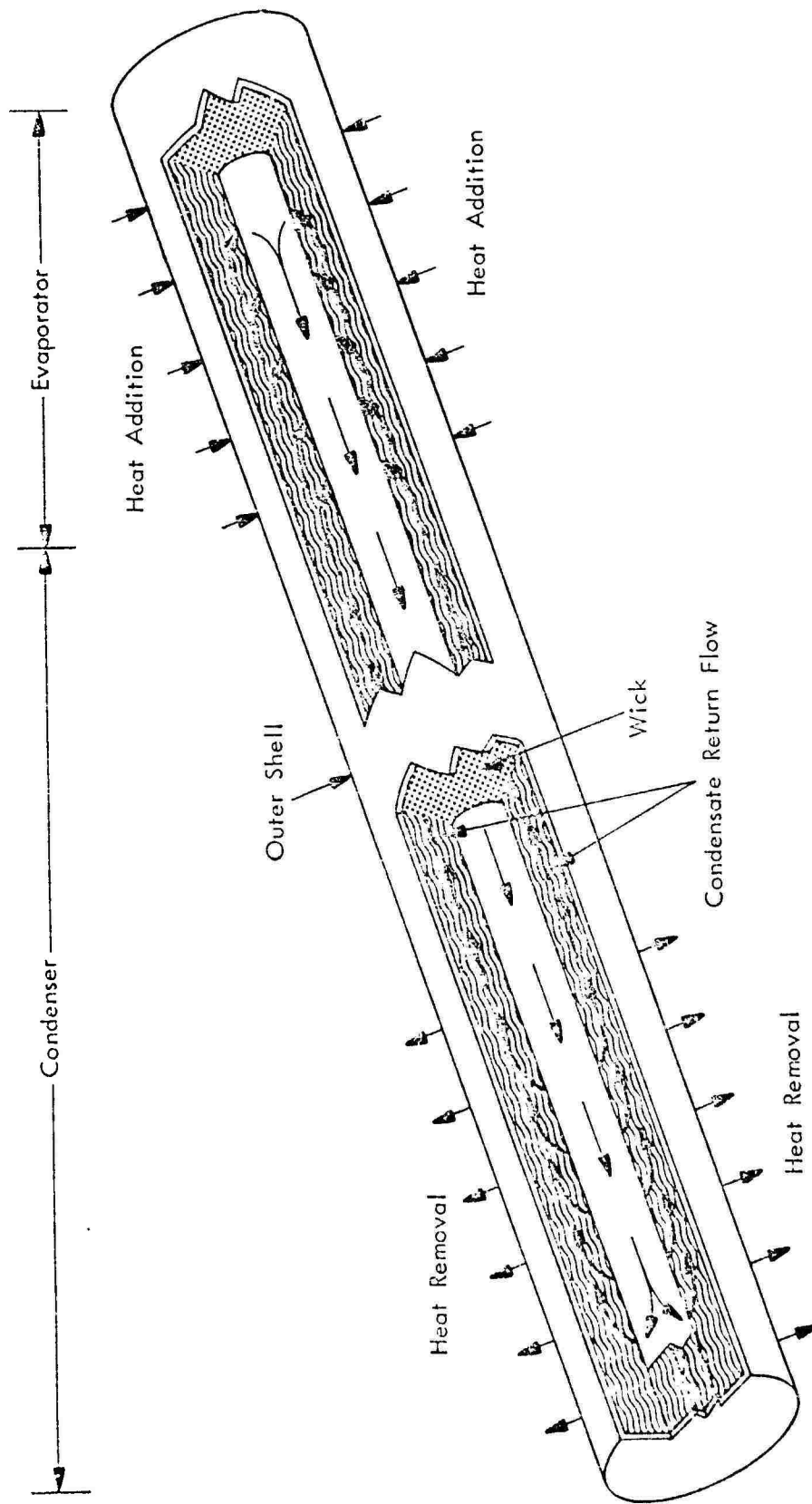
Figure 1 - Parts and Functions of the Basic Heat Pipe
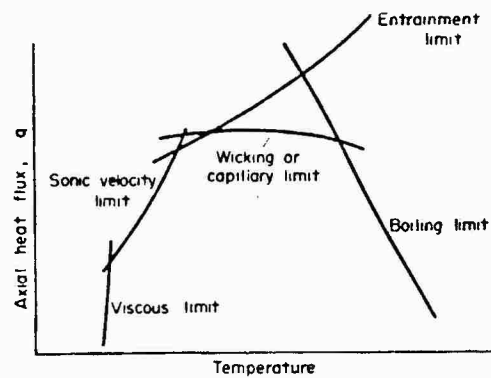
Fig. 2   Limitations to heat transport in the heat pipe
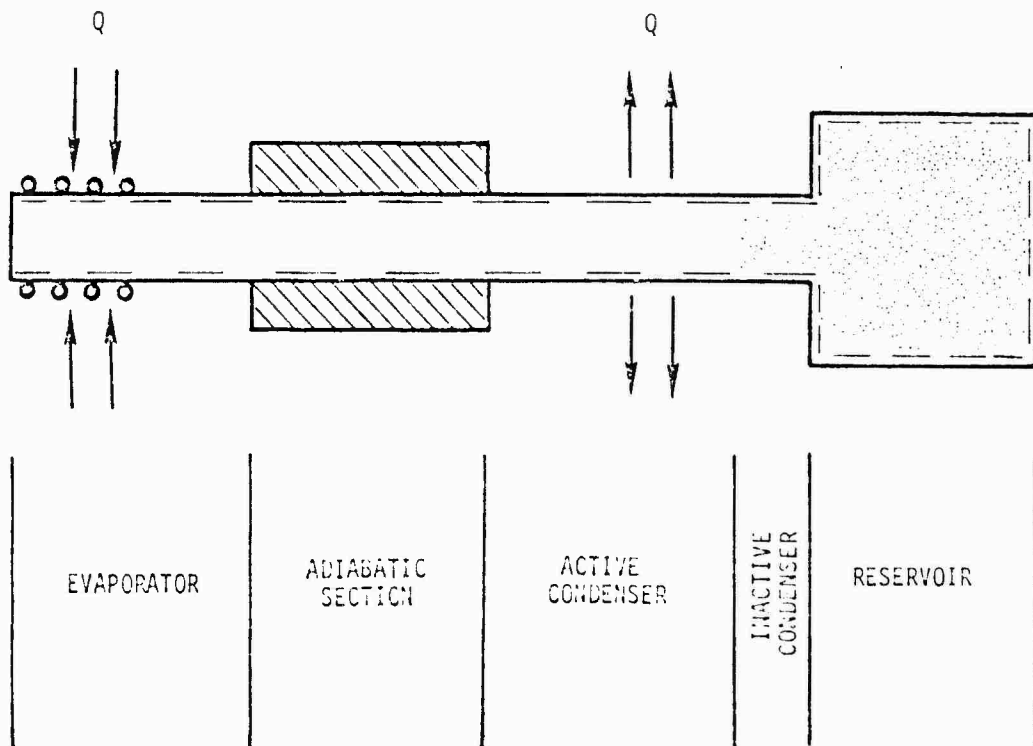
FIG. 3 - NON-CONDENSABLE GAS RESERVOIR VARIABLE
CONDUCTANCE HEAT PIPE
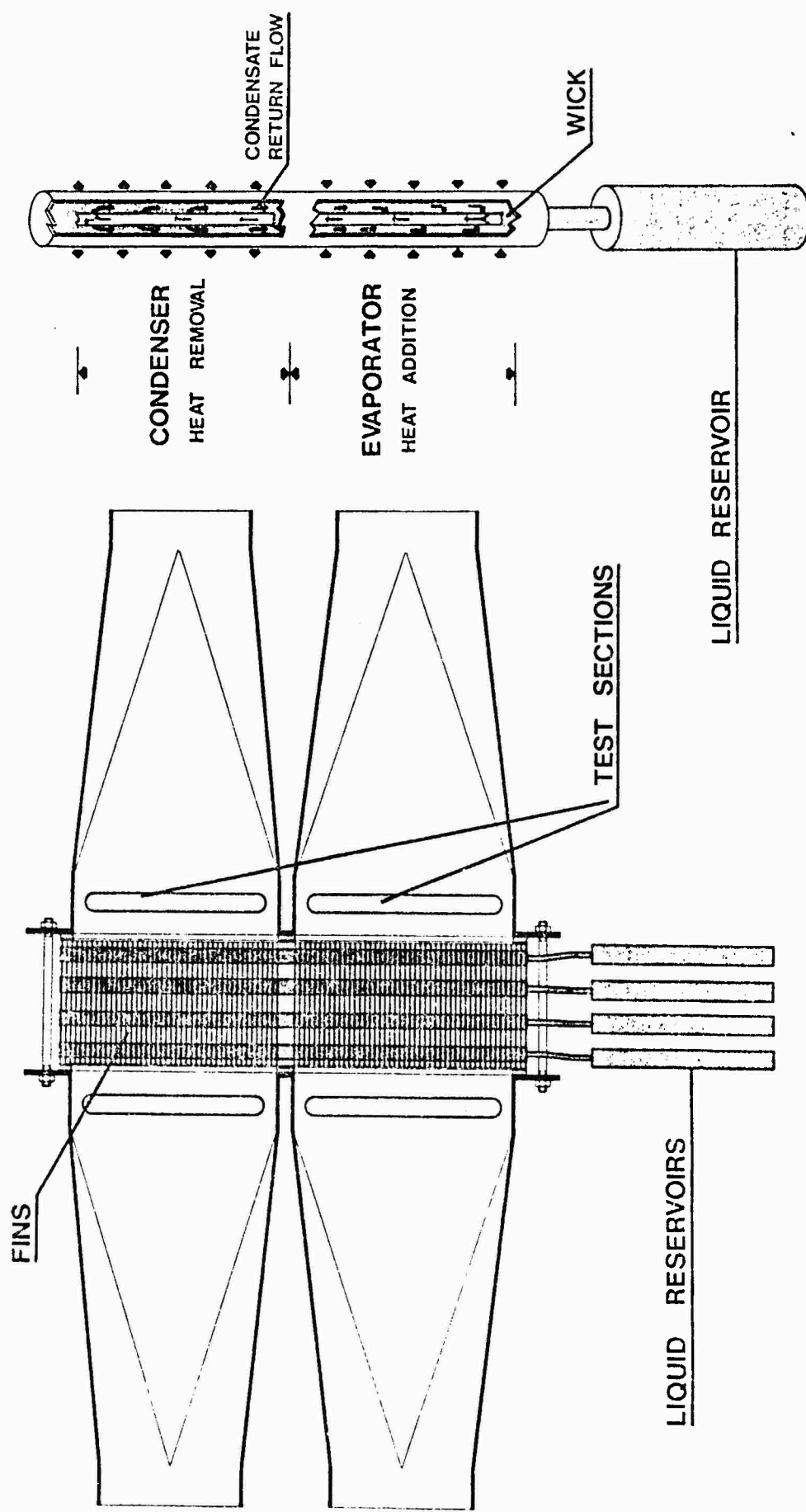
FIG. 4 - Schematic diagram of an air-to-air heat exchanger containing liquid reservoir variable conductance heat pipes.
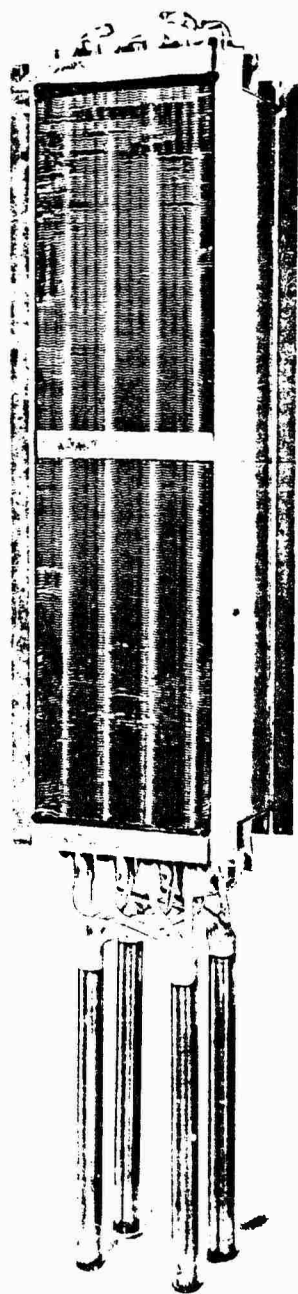
FIG. 5 - THE PROTOTYPE HEAT EXCHANGER

FIG. 6 - THE EXPERIMENTAL FACILITY

COLD AIR INLET

HEATER

ELECTRO-PNEUMATIC VALVES

FLOWMETER

BLOWER

WATER-AIR HEAT EXCHANGER

HOT AIR INLET

BLOWER

FLOWMETER

VALVE

HEAT EXCHANGER

HEATED RESERVOIRS

DATA ACQUISITION SYSTEM
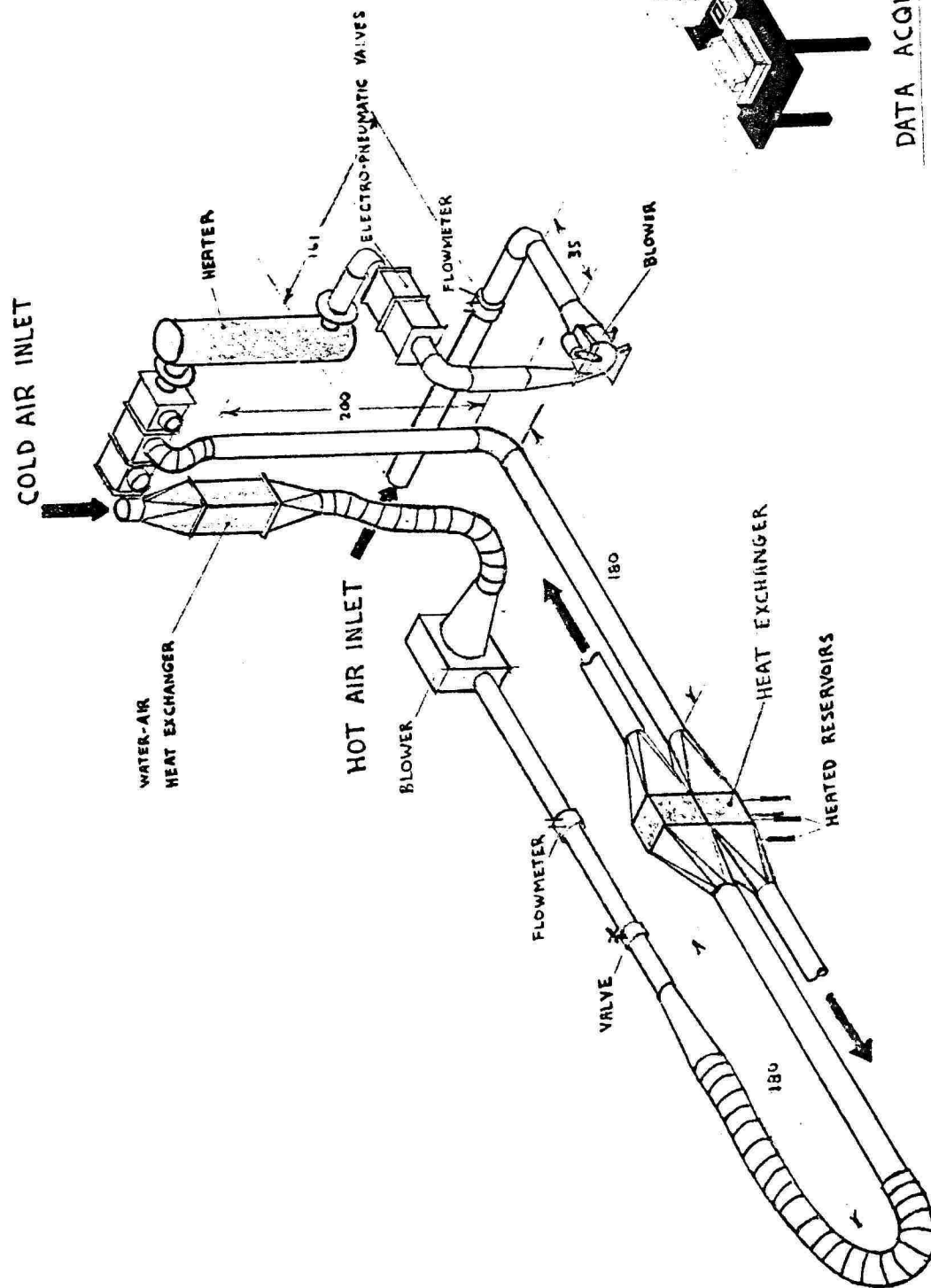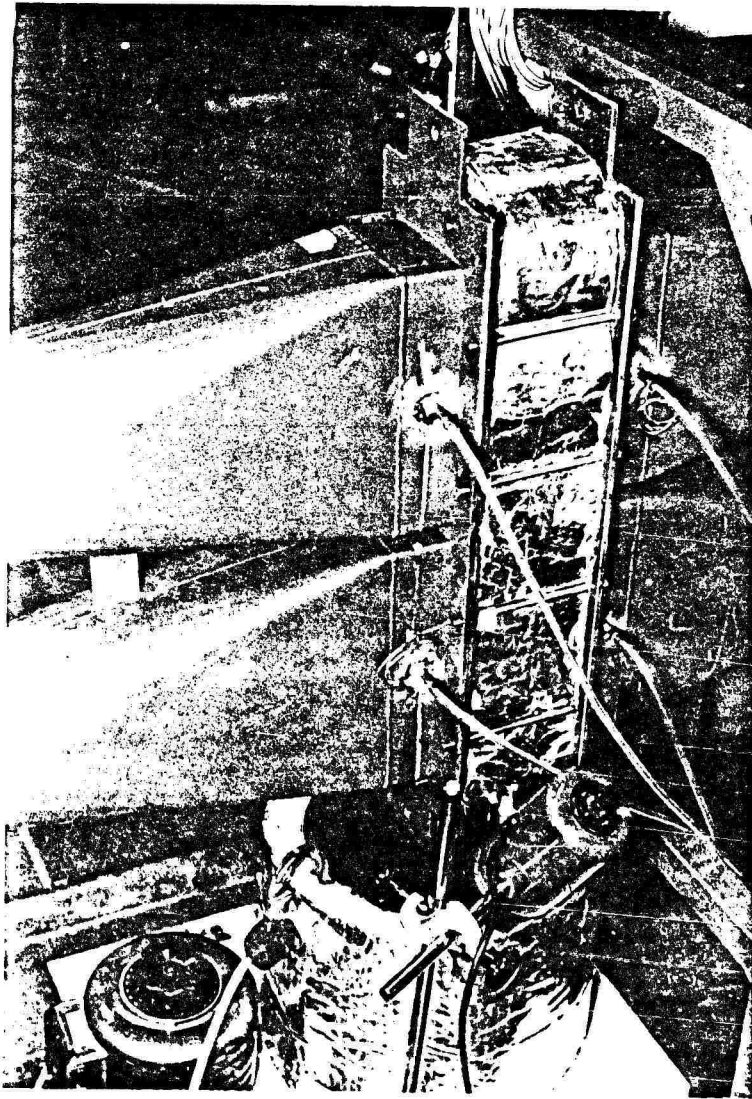
FIG. 7 - REAR VIEW OF HEAT EXCHANGER SHOWING PRESSURE
TAPS, OIL BATH AND ELECTRICAL RESISTANCE HEATER
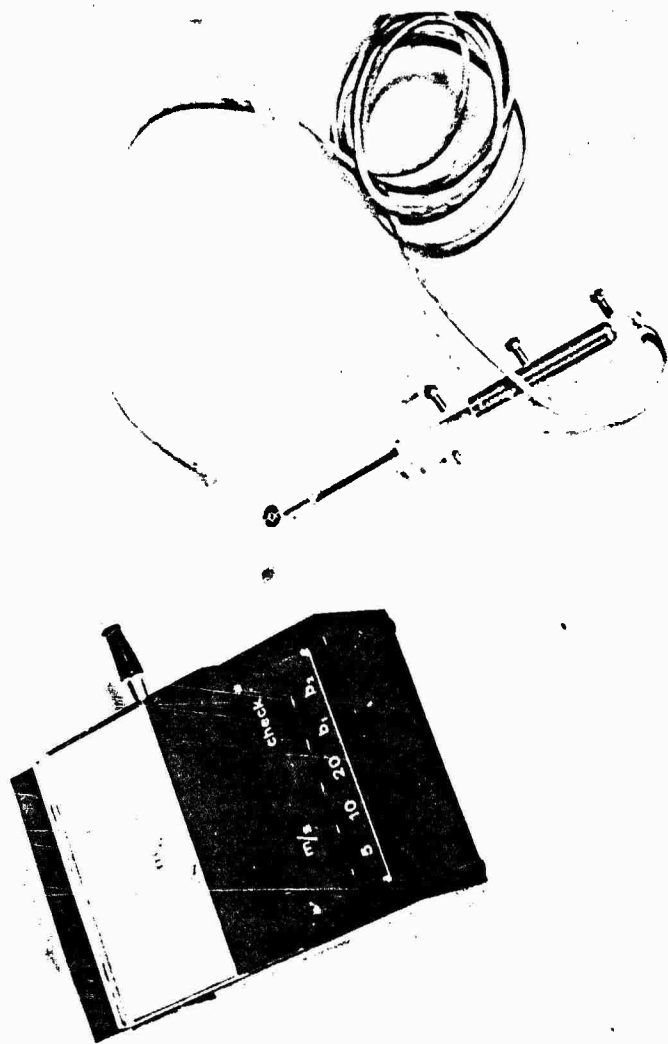
FIG. 8 - VANE ANEMOMETER MOUNTED IN SLIDING SUPPORT
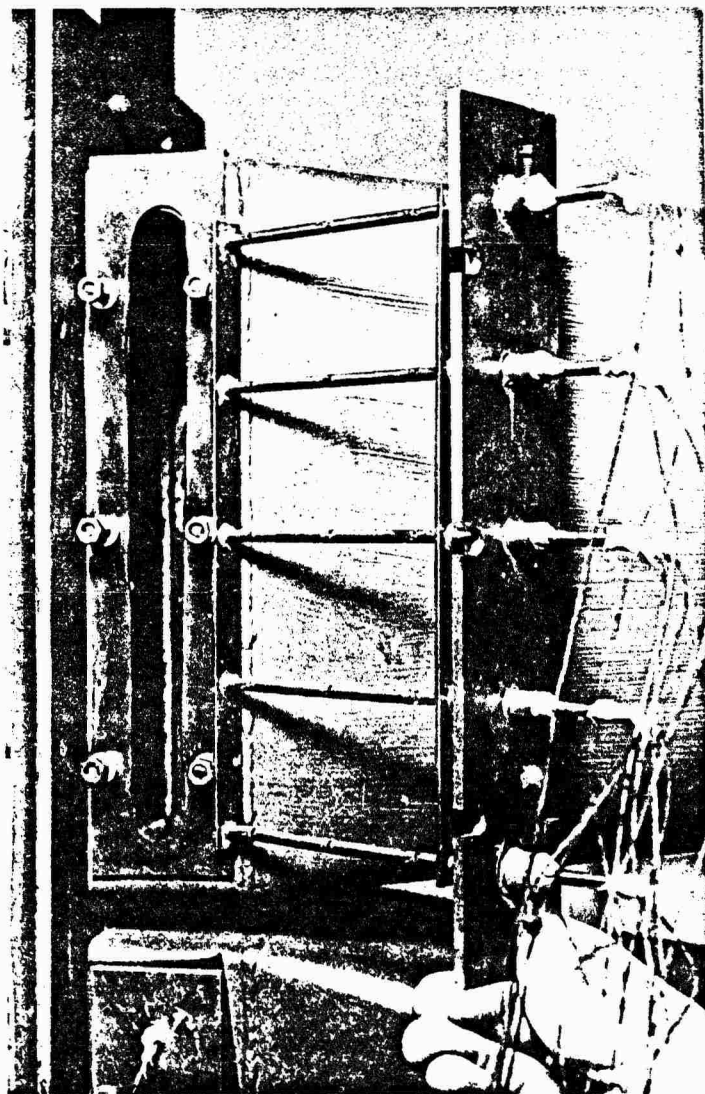
FIG. 9 - THERMOCOUPLE GRID AND TEST SECTION

FIG. 11 – $\dot{m}$ vs. $\sqrt{\Delta p_{HX}}$ FOR THE CONDENSER SECTION

FIG. 10 – $\dot{m}$ vs. $\sqrt{\Delta p_{HX}}$ FOR THE EVAPORATOR SECTION
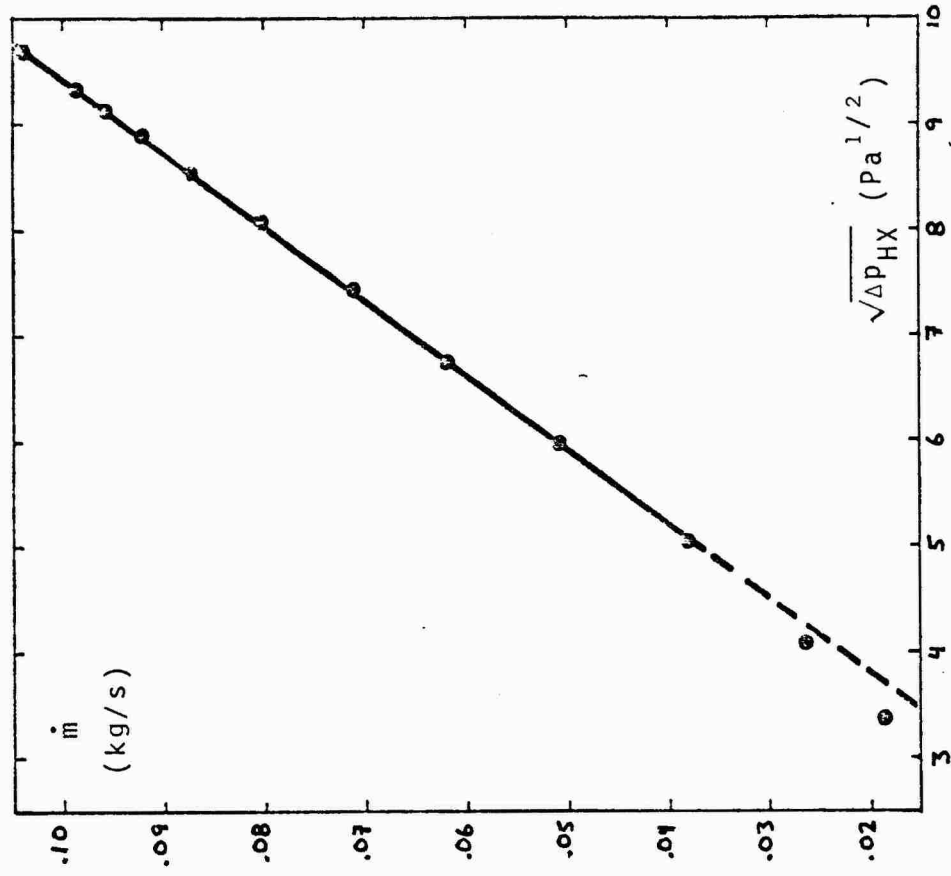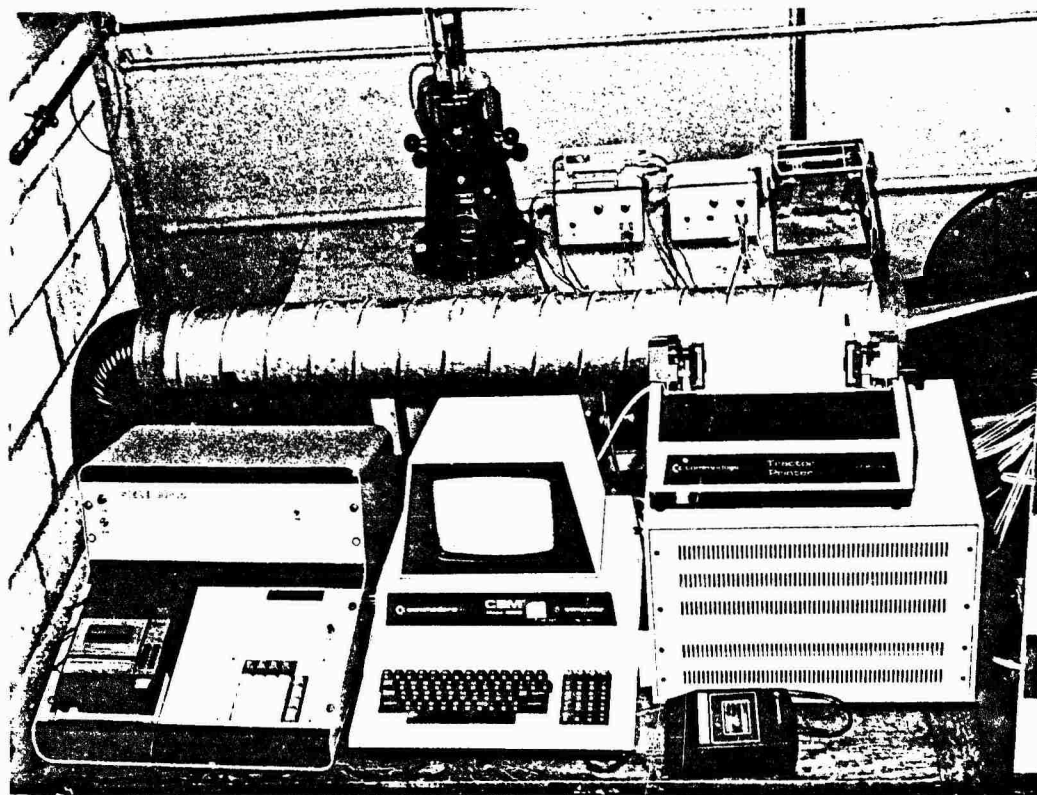
FIG. 12 - CLOSE-UP VIEW OF THE DATA ACQUISITION SYSTEM
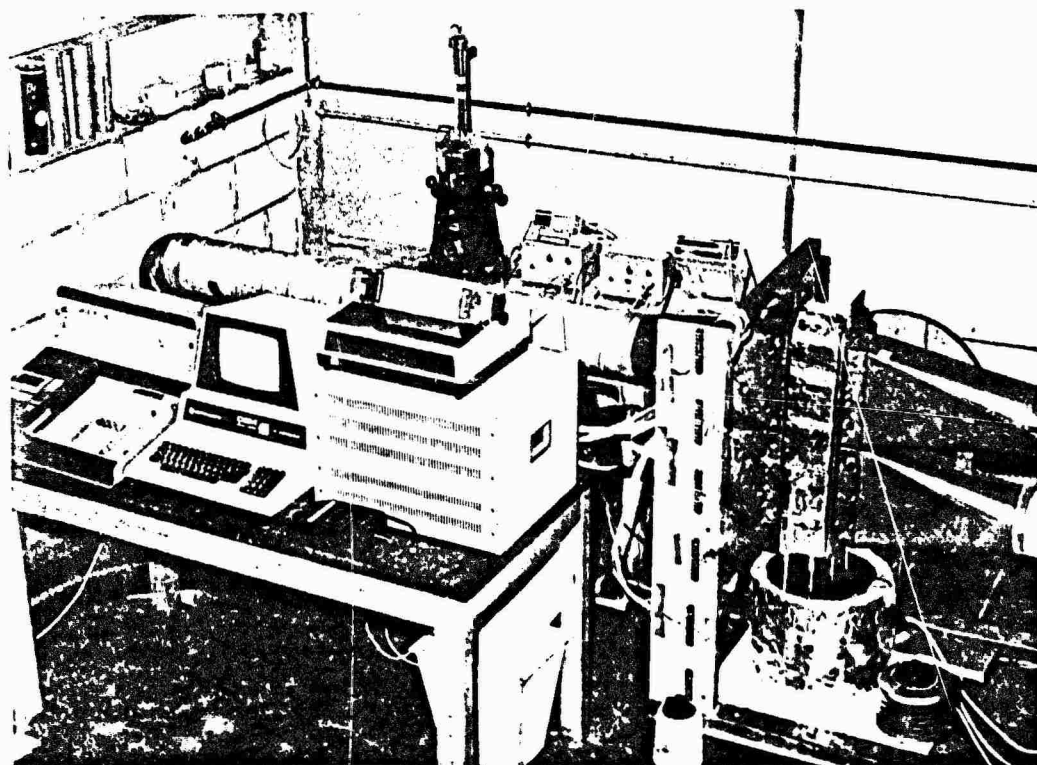
FIG. 13 - VIEW OF THE INSTRUMENTED HEAT EXCHANGER AND THE
DATA ACQUISITION SYSTEM
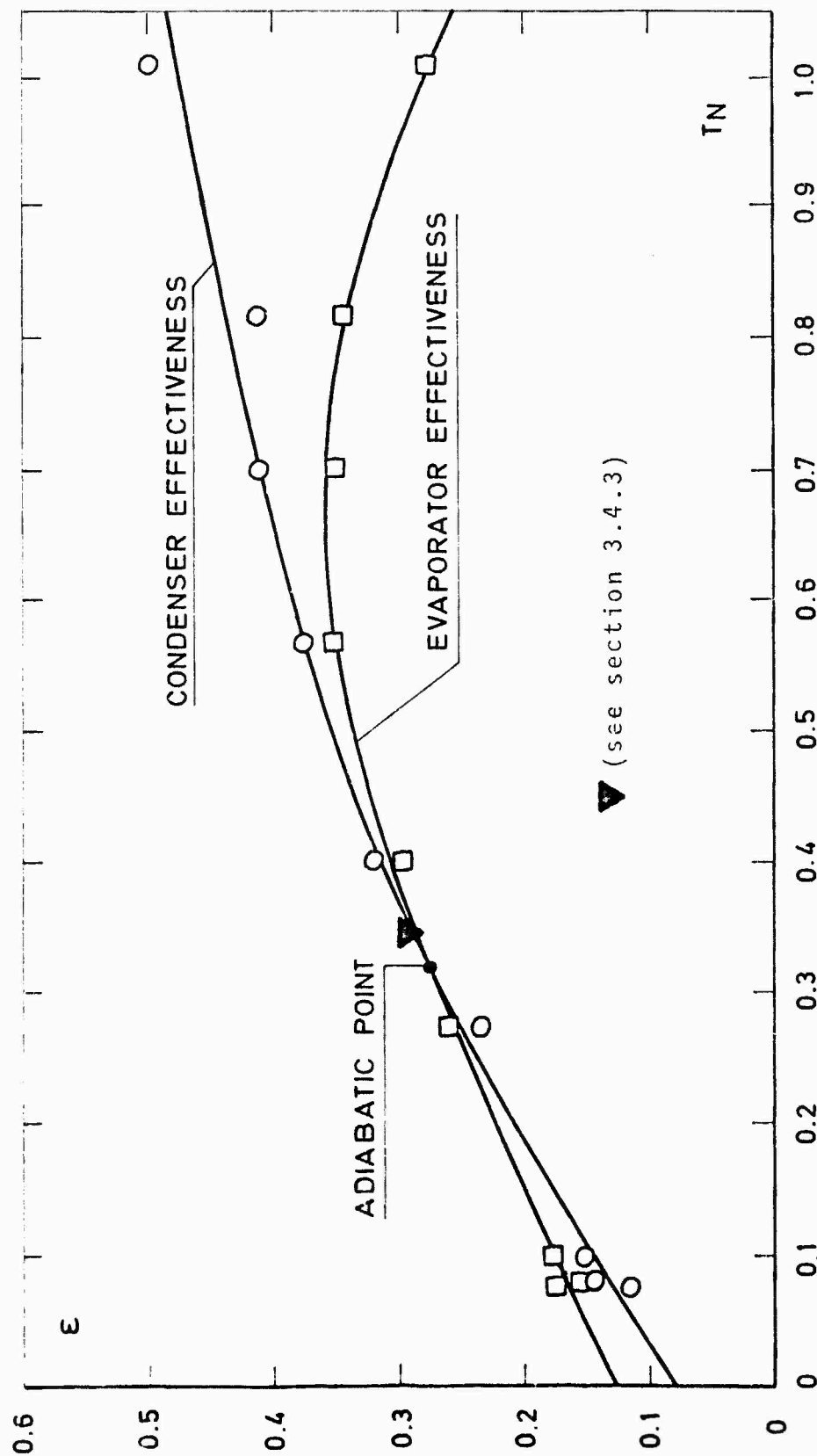
FIG. 14 - EVAPORATOR AND CONDENSER EFFECTIVENESS vs. NORMALIZED RESERVOIR TEMPERATURE FOR MASS FLOW RATIO = 1.0

FIG. 15 – TYPICAL OUTLET AIR TEMPERATURE PROFILE IN THE SUB-ADIABATIC REGIME

Test Conditions

heater power = 6 kW

MR = 1.0

T_n = 0.19

ε_{HX} = 0.19
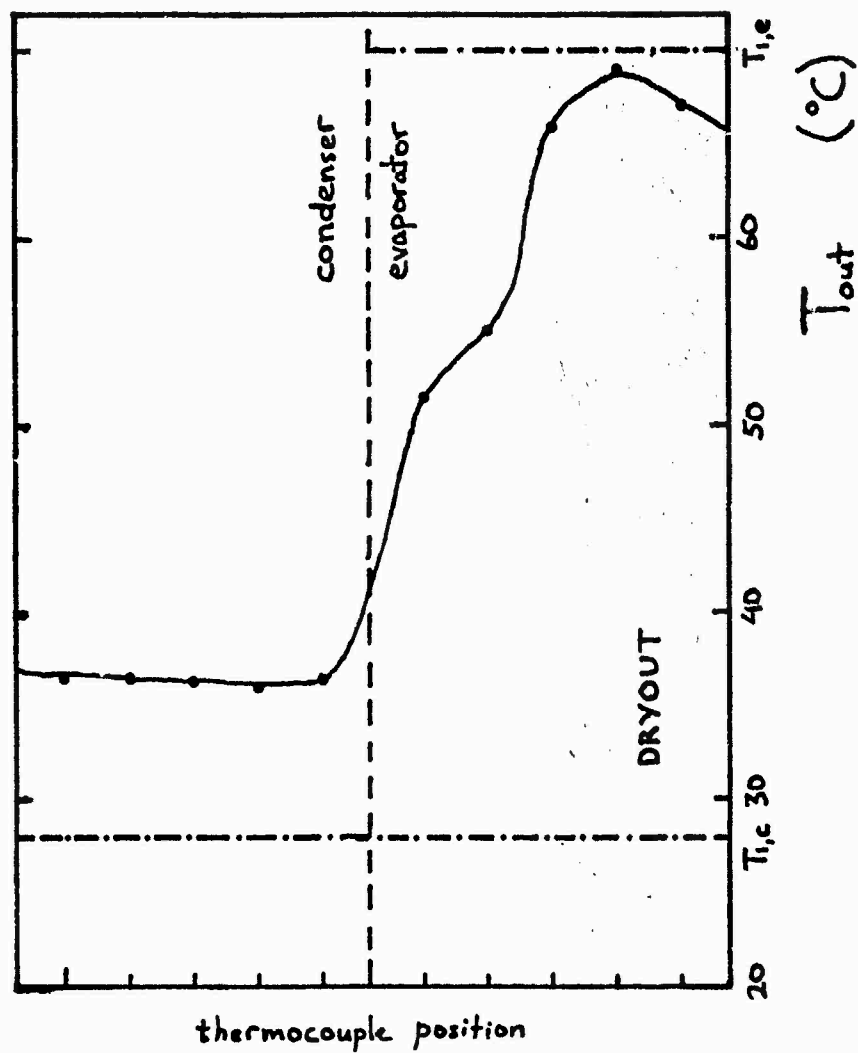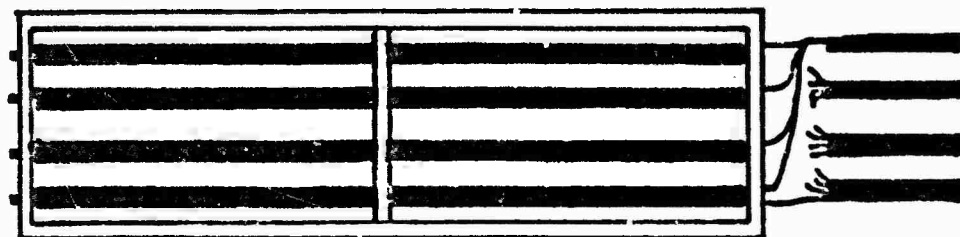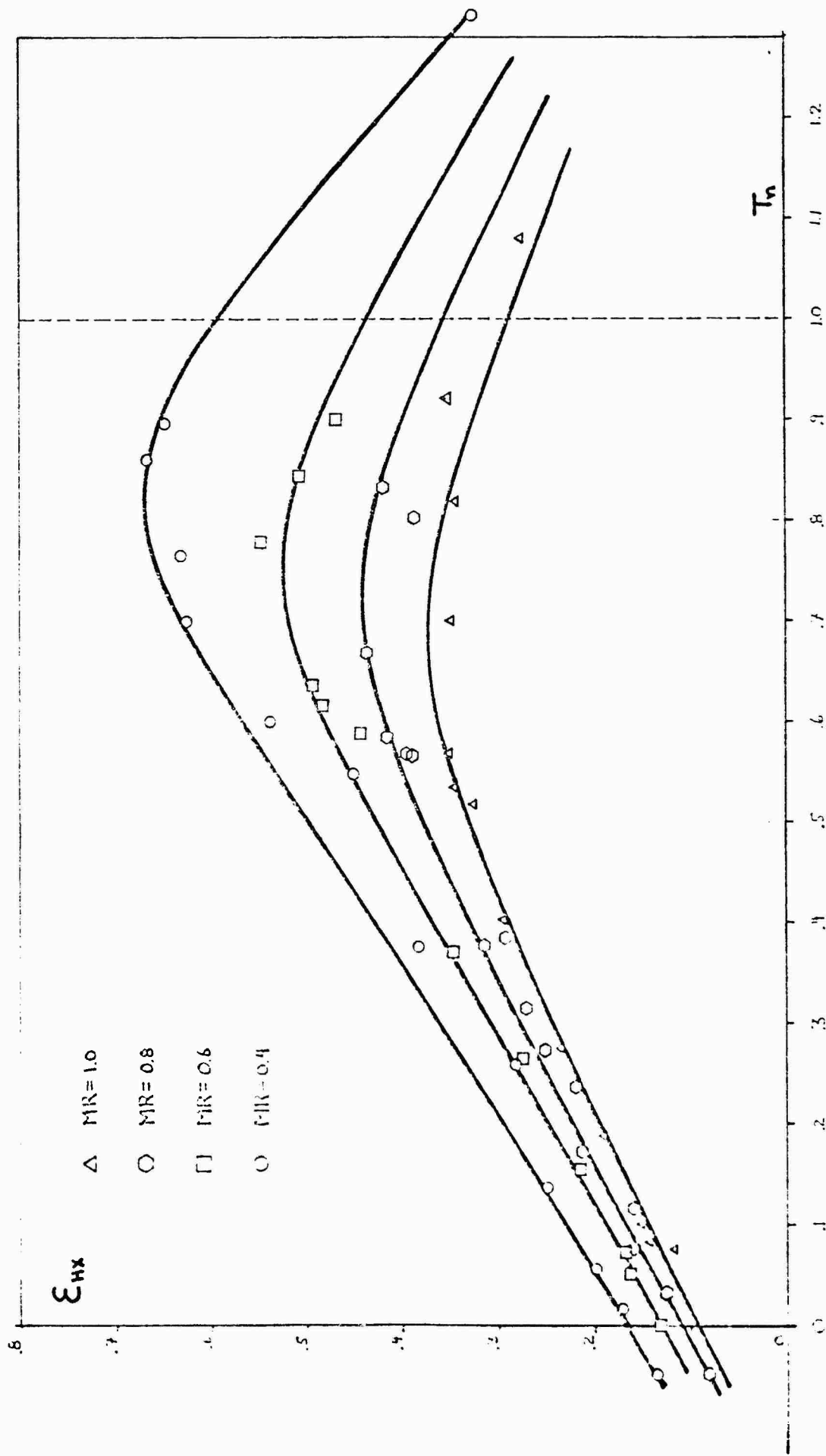
FIG. 16 - TRUE HEAT EXCHANGER EFFECTIVENESS vs. NORMALIZED RESERVOIR TEMPERATURE FOR VARIOUS MASS FLOW RATIOS

FIG. 17 - DISCRETIZATION OF THE HEAT EXCHANGER INTO PLATELETS AND HEAT SOURCE/SINKS
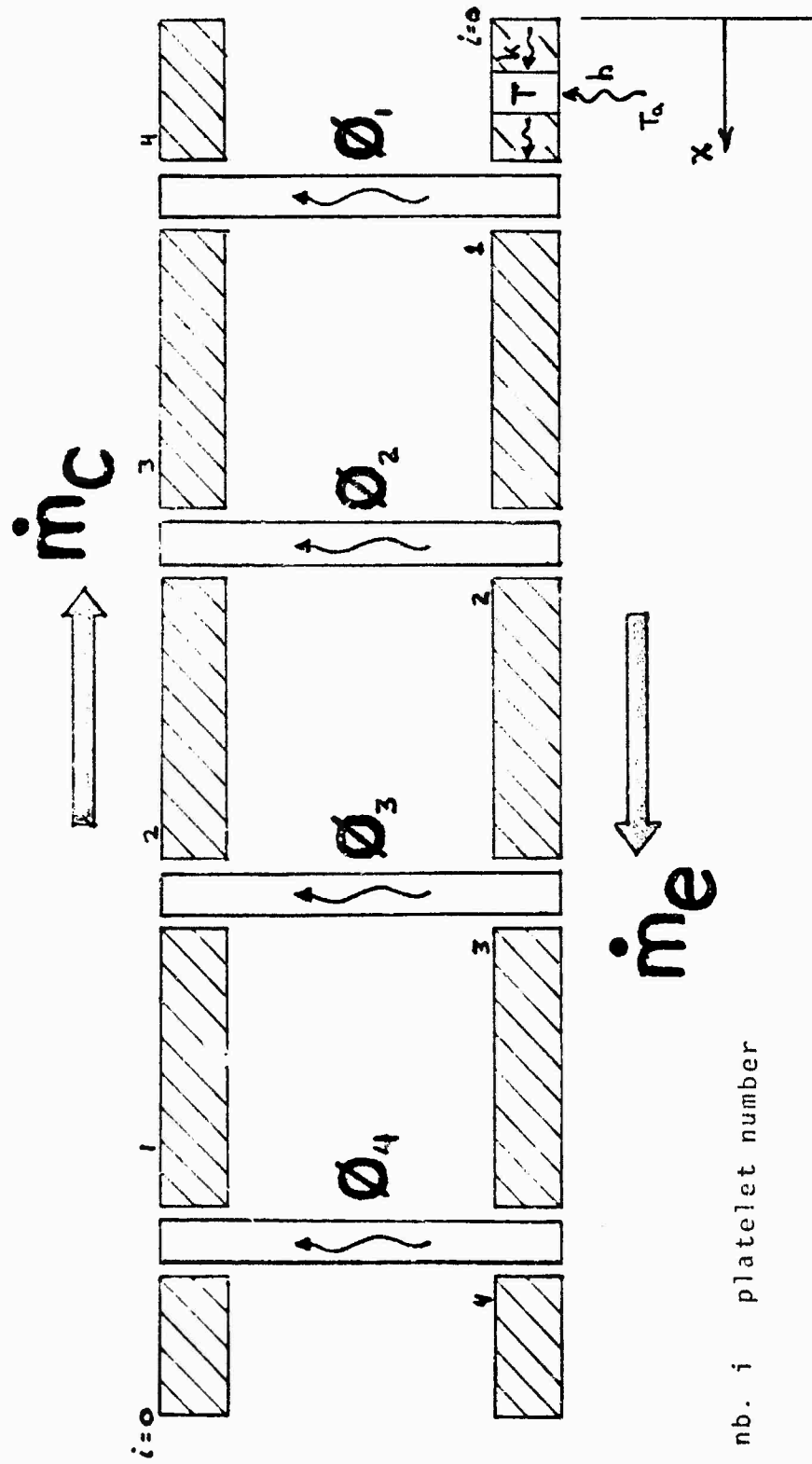
nb. i   platelet number
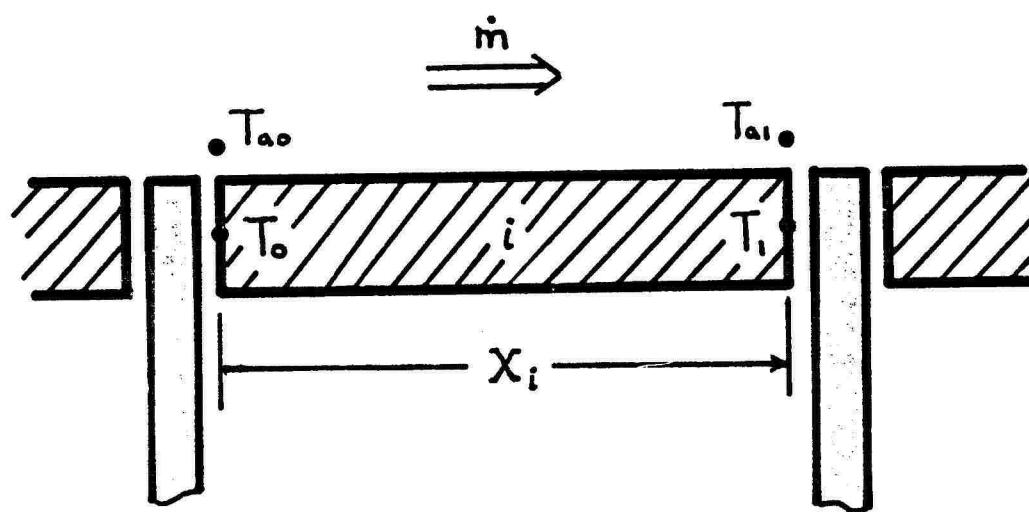
FIG. 18 - NOMENCLATURE FOR A SINGLE PLATELET (§ 4.4)

$$\underline{\underline{A}}\,\underline{T} = \underline{\underline{B}}\,T_{a\infty} + \underline{\underline{C}}\,\underline{\alpha}$$

Matrix columns/vectors labelled:

$T_0,\ T_1,\ T_2,\ T_3,\ T_4,\ T_5,\ T_{a0},\ T_{a1},\ T_{a2},\ T_{a3},\ T_{a4},\ T_{a5}$

$= \quad 1 \quad T_{a\infty} \quad + \quad \varphi_1,\ \varphi_2,\ \varphi_3,\ \varphi_4 \quad \alpha$

nb. Subscript numbers refer to nodes

FIG. 20 - SEVERAL IDEALIZED LIQUID PROFILES IN THE WICK
(CROSS-SECTIONAL VIEW OF THE HEAT PIPE WALL)
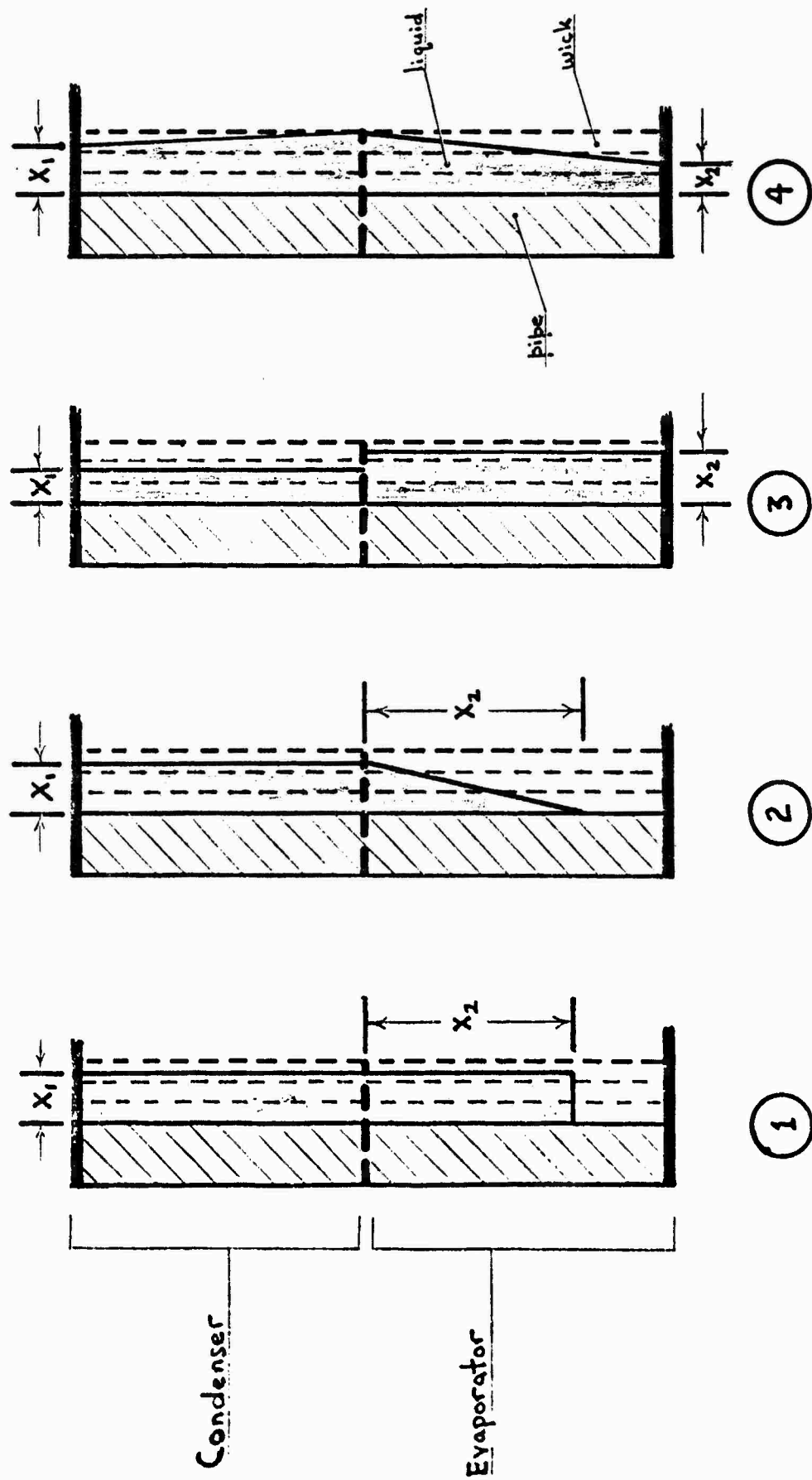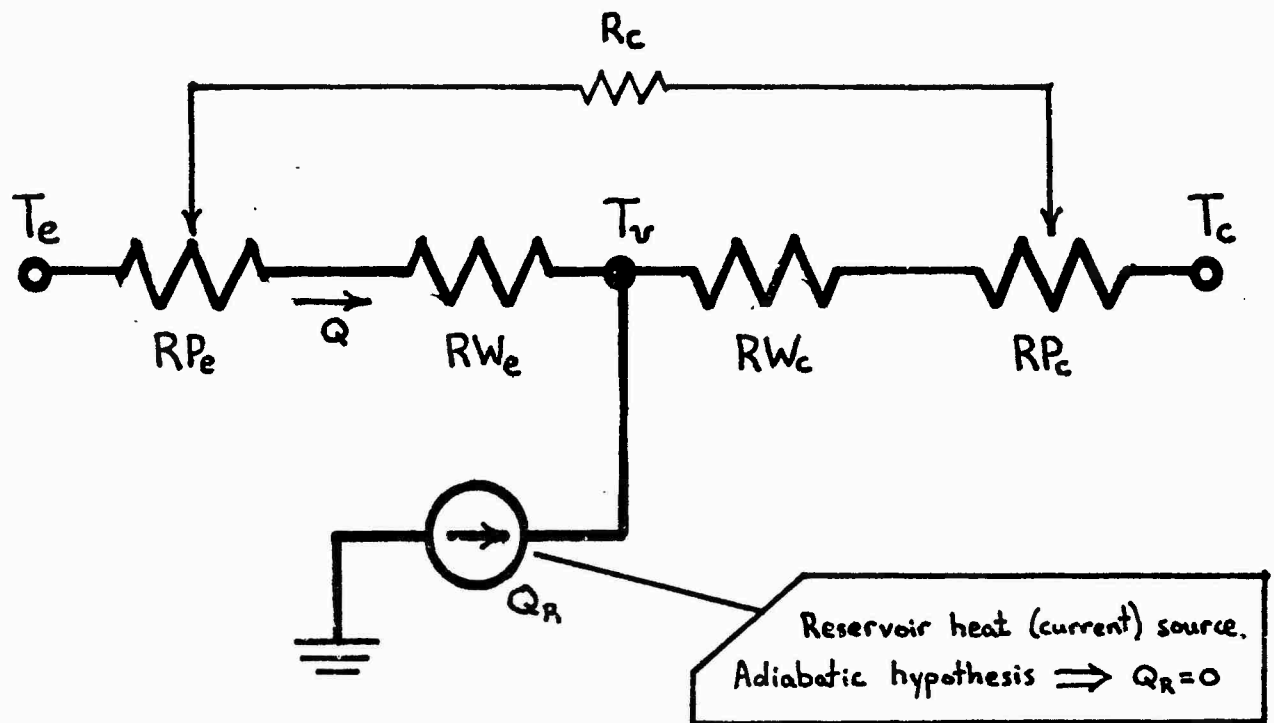
FIG. 21 - THERMAL RESISTANCE NETWORK MODEL OF THE HEAT PIPE
(see section 4.2.2)
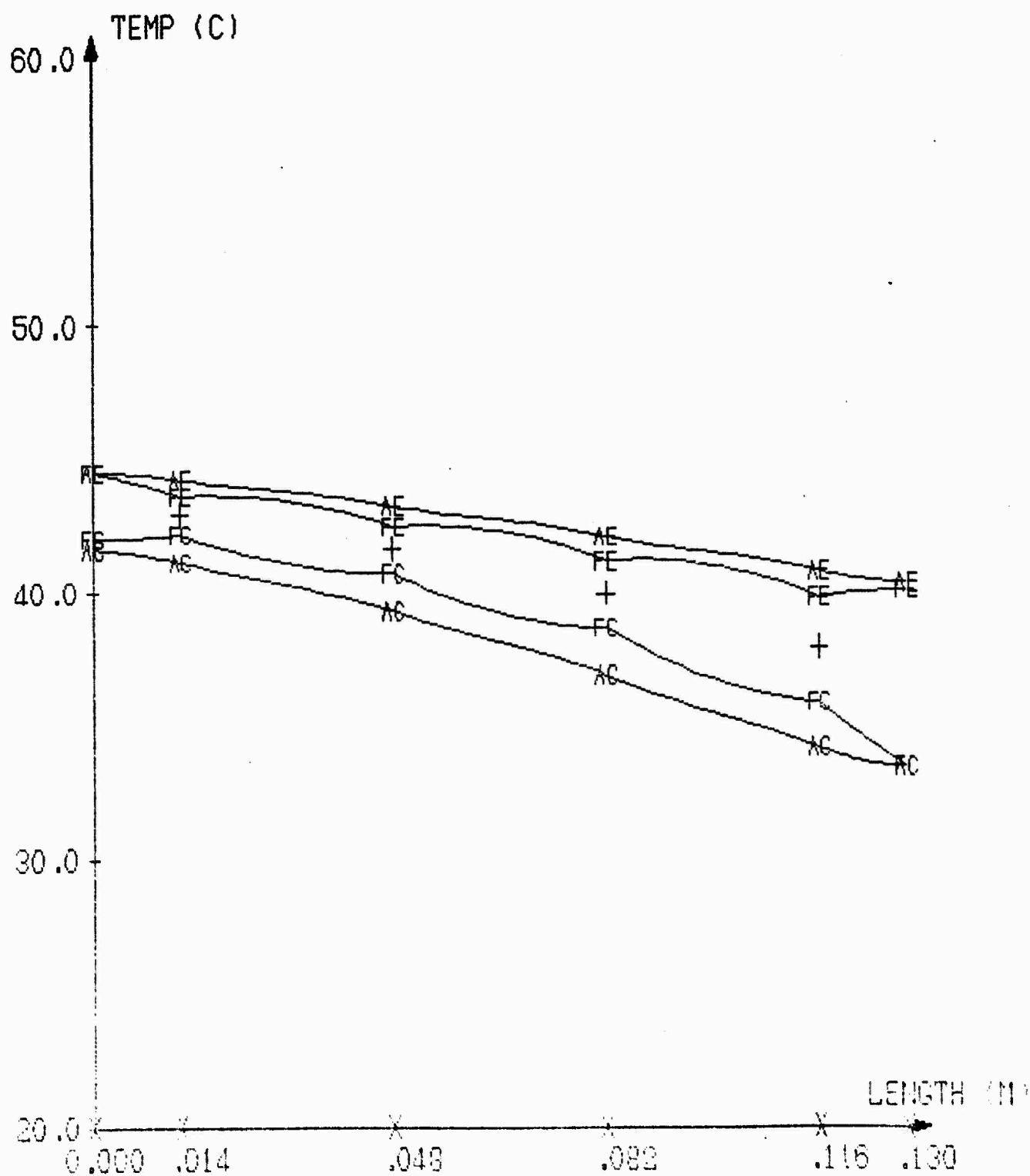
FIG. 22 AIR (A) AND FIN (F) TEMPERATURE PROFILES IN THE
EVAPORATOR (E) AND CONDENSER (C) SECTIONS OF AN
HEAT PIPE HEAT EXCHANGER.
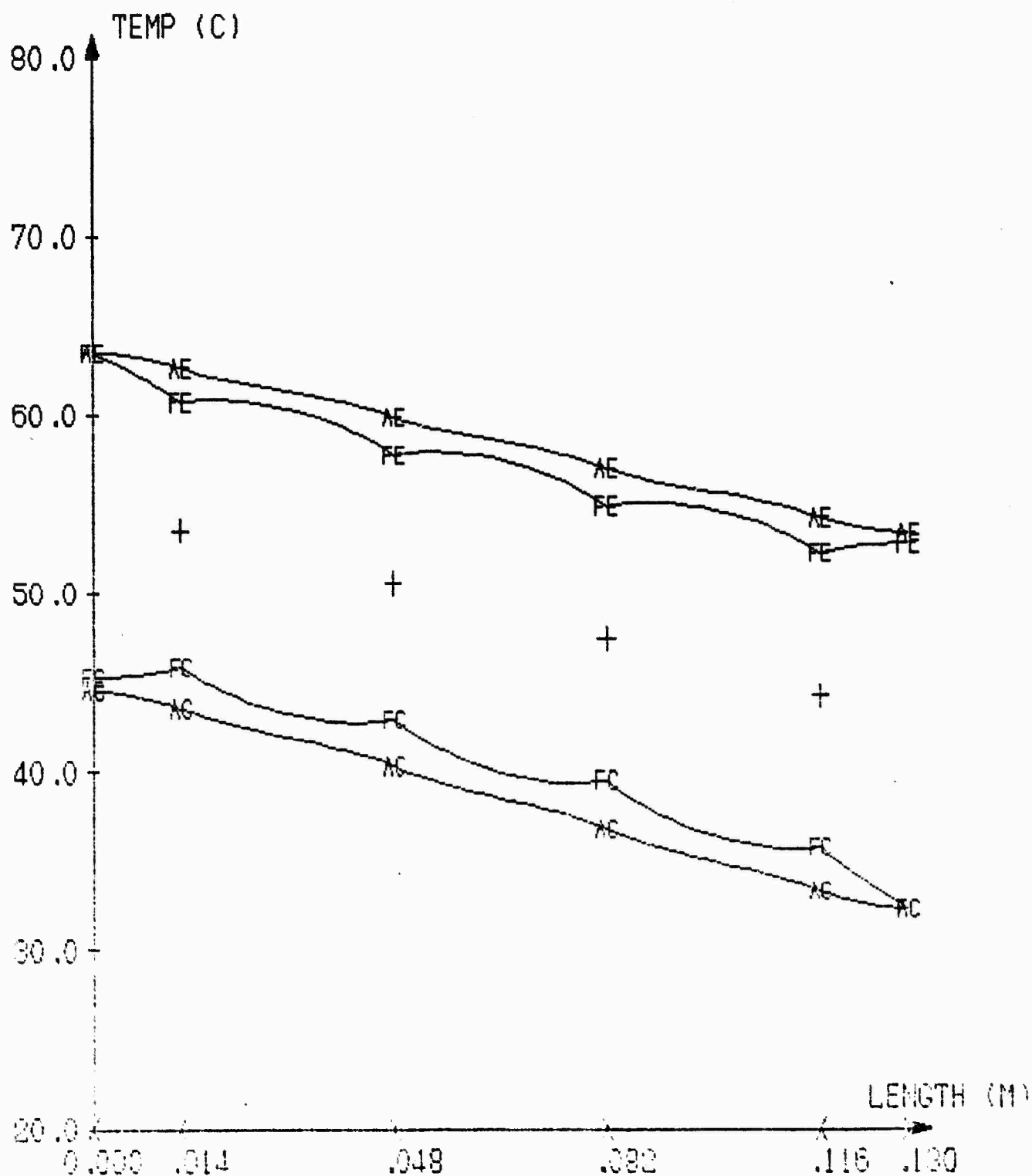(+) HEAT PIPE VAPOR TEMPERATURE
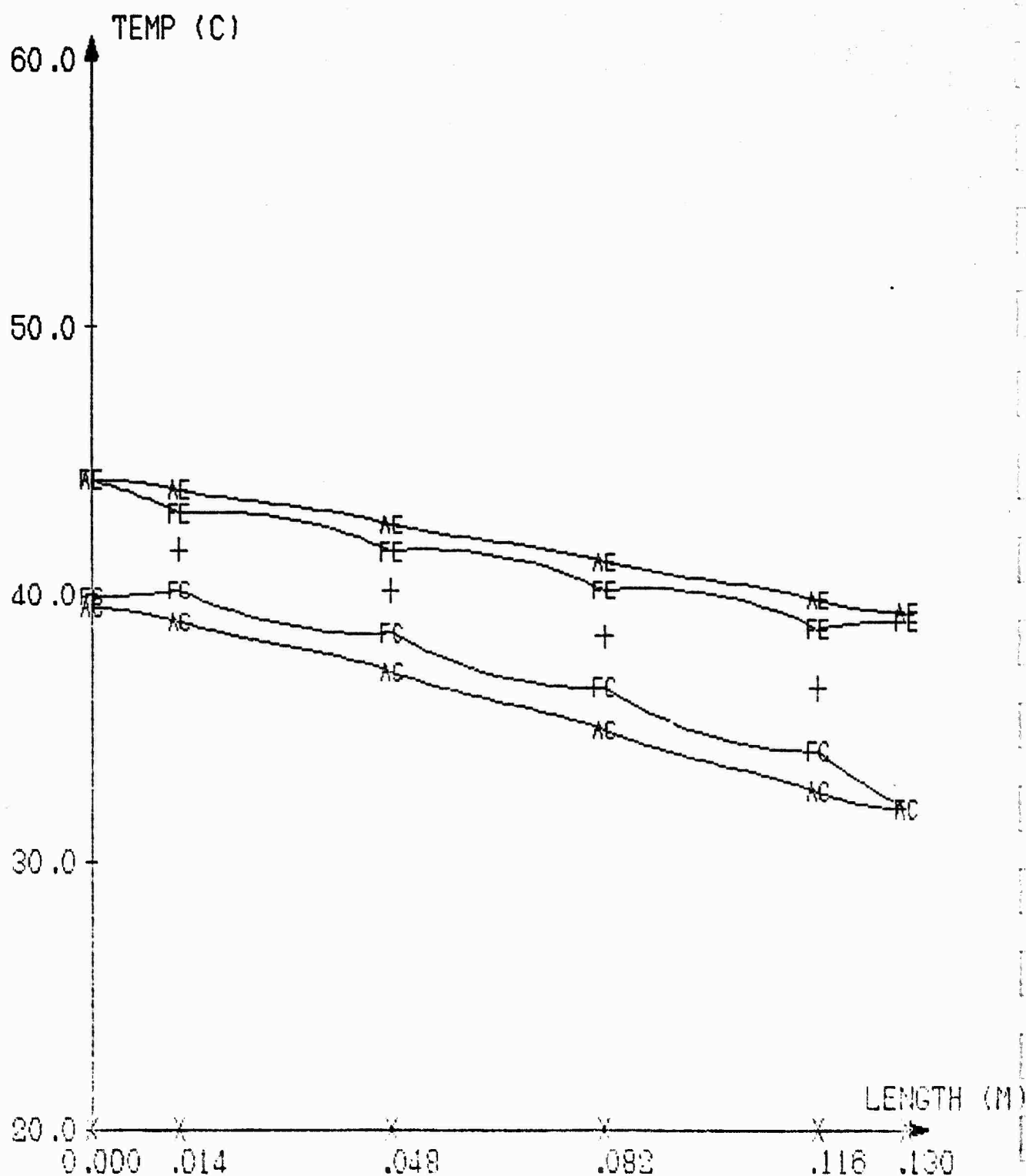
FIG. 23   AIR (A) AND FIN (F) TEMPERATURE PROFILES IN THE
EVAPORATOR (E) AND CONDENSER (C) SECTIONS OF AN
HEAT PIPE HEAT EXCHANGER.

(+) HEAT PIPE VAPOR TEMPERATURE
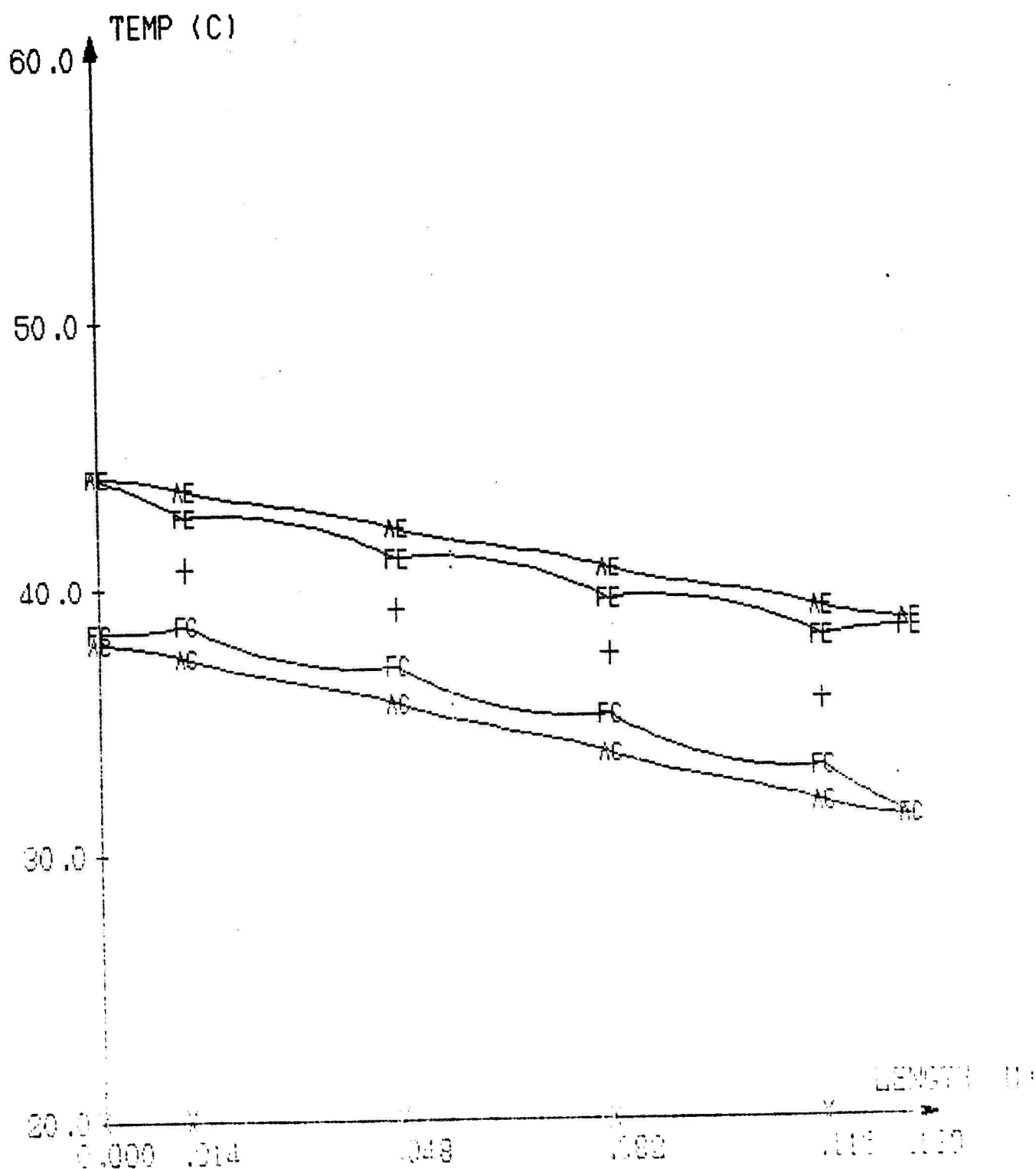
FIG. 24 AIR (A) AND FIN (F) TEMPERATURE PROFILES IN THE
EVAPORATOR (E) AND CONDENSER (C) SECTIONS OF AN
HEAT PIPE HEAT EXCHANGER.

(+) HEAT PIPE VAPOR TEMPERATURE

AIR INLET TEMPERATURES 45 C, 30 C ; MASS FLOW RATIO .8
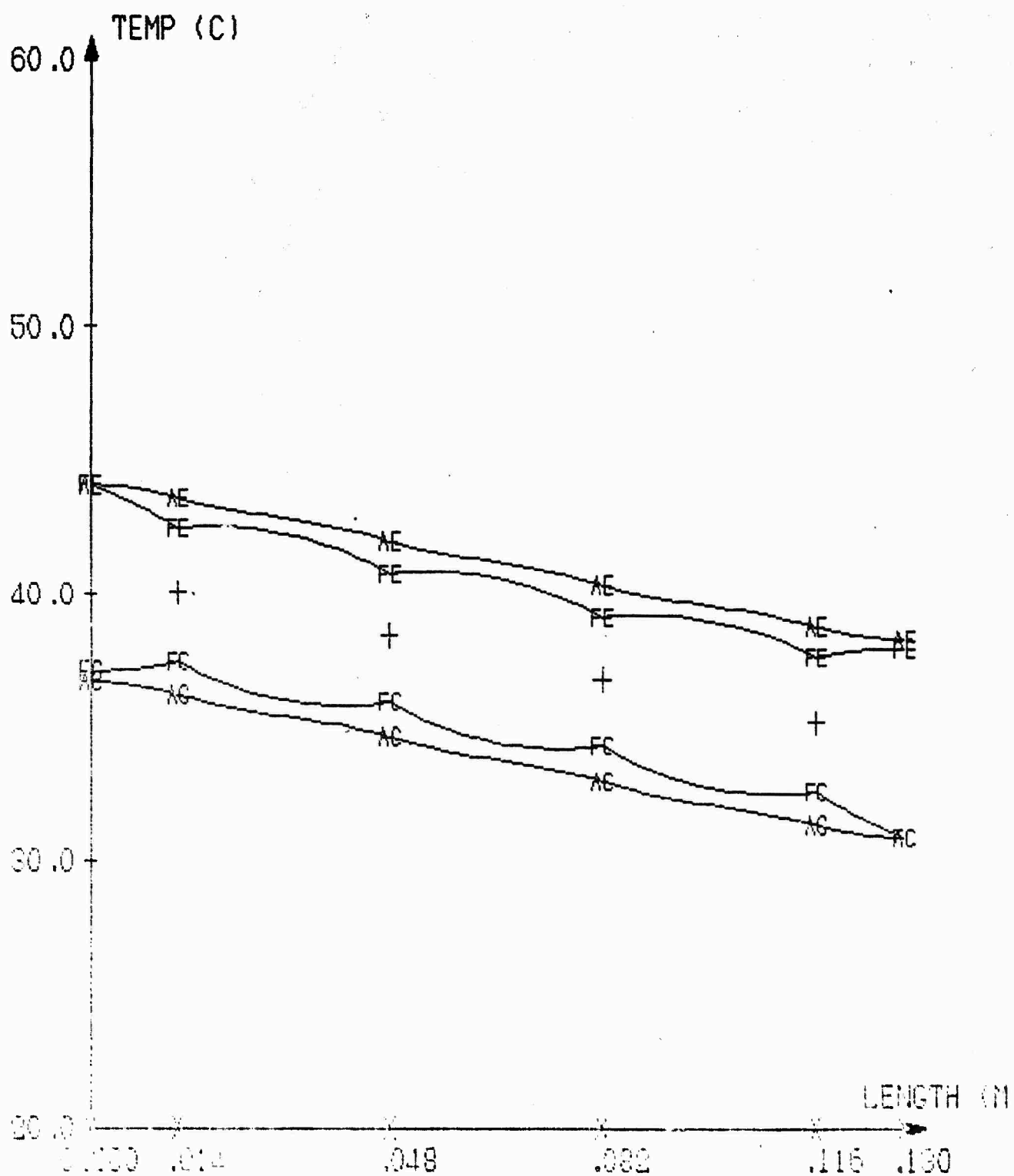
FIG. 25   AIR (A) AND FIN (F) TEMPERATURE PROFILES IN THE

EVAPORATOR (E) AND CONDENSER (C) SECTIONS OF AN

HEAT PIPE HEAT EXCHANGER.

(+) HEAT PIPE VAPOR TEMPERATURE

AIR INLET TEMPERATURES 45 C, 30 C, MASS FLOW RATIO 1
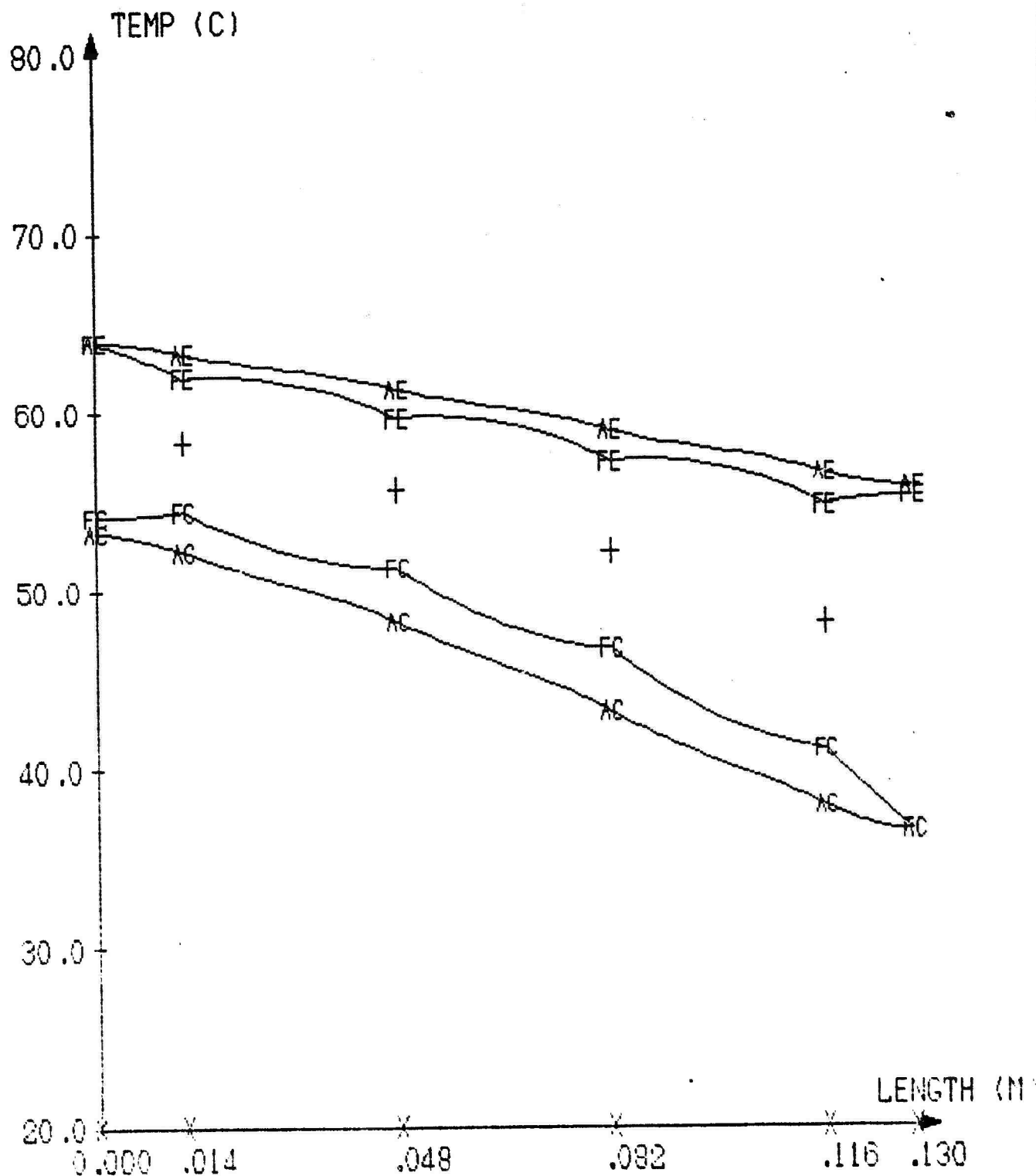
FIG. 26   AIR (A) AND FIN (F) TEMPERATURE PROFILES IN THE
EVAPORATOR (E) AND CONDENSER (C) SECTIONS OF AN
HEAT PIPE HEAT EXCHANGER.

(+) HEAT PIPE VAPOR TEMPERATURE

AIR INLET TEMPERATURES 65 C. 30 C ; MASS FLOW RATIO .4
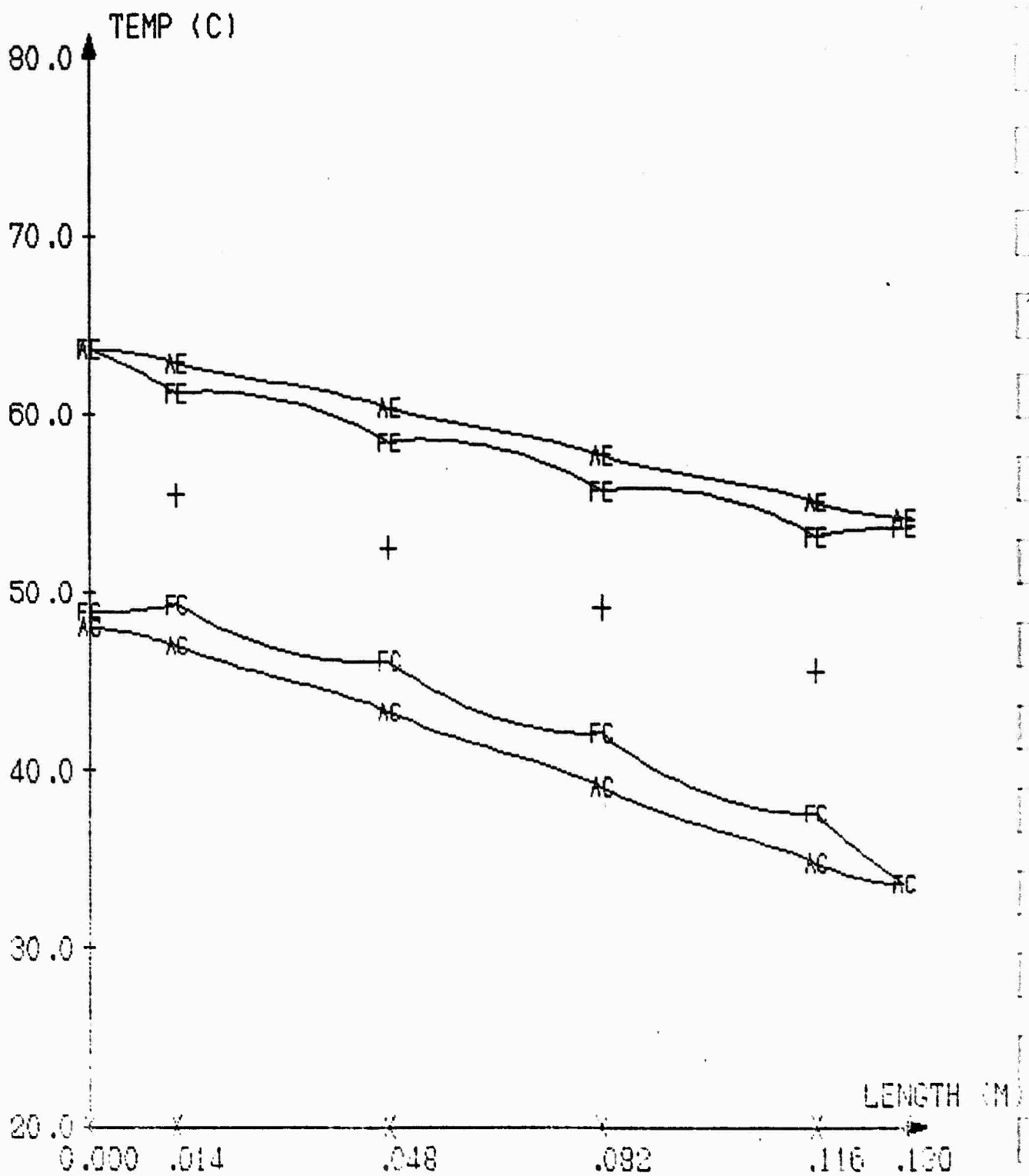
FIG. 27 AIR (A) AND FIN (F) TEMPERATURE PROFILES IN THE
EVAPORATOR (E) AND CONDENSER (C) SECTIONS OF AN
HEAT PIPE HEAT EXCHANGER.

(+) HEAT PIPE VAPOR TEMPERATURE

FIG. 28 AIR (A) AND FIN (F) TEMPERATURE PROFILES IN THE
EVAPORATOR (E) AND CONDENSER (C) SECTIONS OF AN
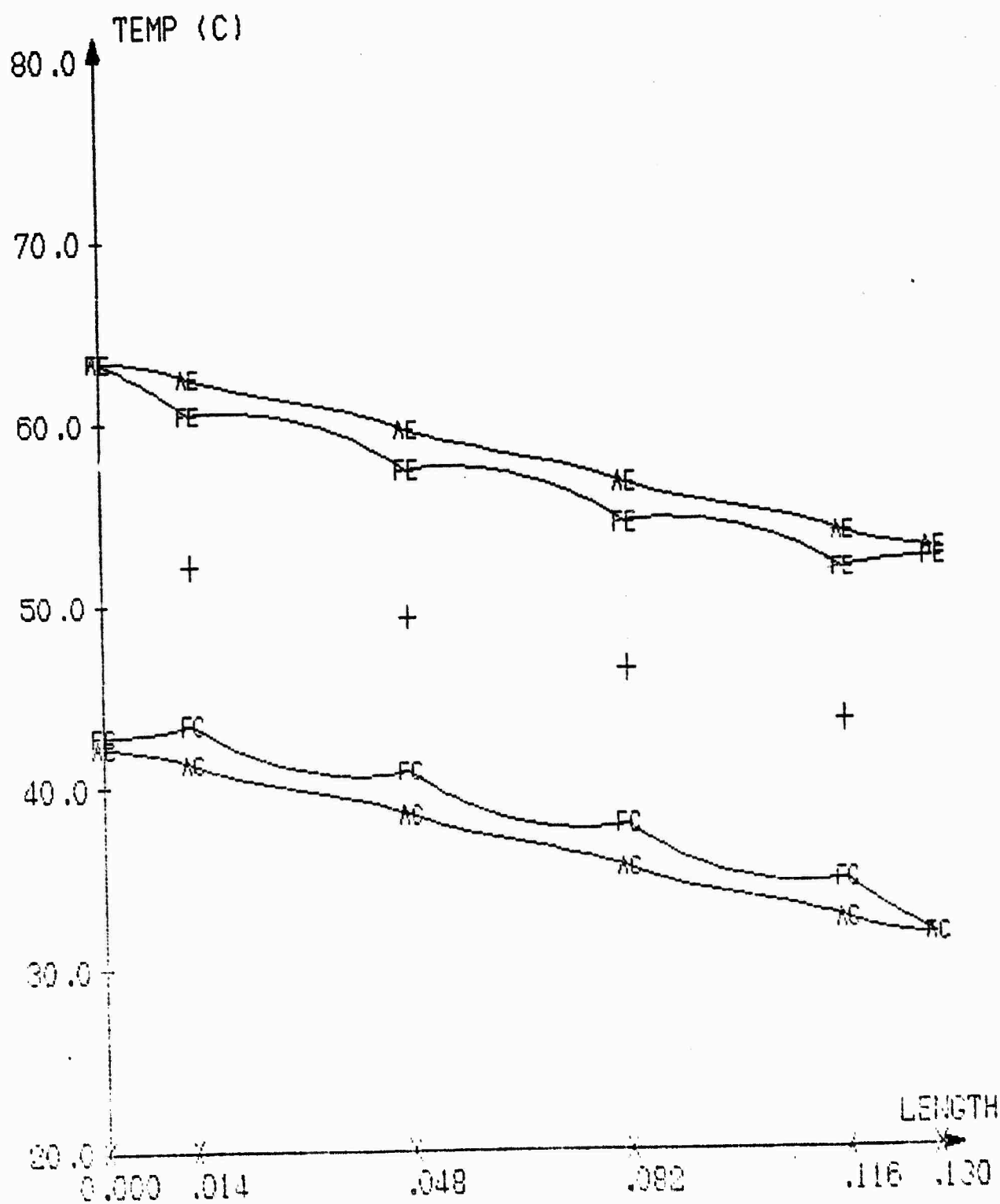HEAT PIPE HEAT EXCHANGER.

(+) HEAT PIPE VAPOR TEMPERATURE

FIG. 29 AIR (A) AND FIN (F) TEMPERATURE PROFILES IN THE
EVAPORATOR (E) AND CONDENSER (C) SECTIONS OF AN
HEAT PIPE HEAT EXCHANGER.
(+) HEAT PIPE VAPOR TEMPERATURE
AIR INLET TEMPERATURES 65 C, 30 C ; MASS FLOW RATIO 1.

FIG. 30 - COMPARISON OF COMPUTATIONAL AND EXPERIMENTAL RESULTS : TRUE HEAT
EXCHANGER EFFECTIVENESS vs. NORMALIZED RESERVOIR TEMPERTURE